Recent extensions and applications of the 'CST' universal parametric geometry representation method

B. M. Kulfan
brenda.m.kulfan@boeing.com
Boeing Commercial Airplanes,
Seattle, Washington
USA

ABSTRACT

For aerodynamic design optimisation as well as for multidisciplinary design optimisation studies, it is very desirable to limit the number of the geometric design variables. In Ref. 1, a 'fundamental' parametric aerofoil geometry representation method was presented. The method included the introduction of a geometric 'class function/shape function' transformation technique, CST, such that round nose/sharp aft end geometries as well as other classes of geometries could be represented exactly by analytic well behaved and simple mathematical functions having easily observed physical features. The CST method was shown to describe an essentially limitless design space composed entirely of analytically smooth geometries. In Ref. 2, the CST methodology was extended to more general three dimensional applications such as wing, body, ducts and nacelles. It was shown that any general 3D geometry can be represented by a distribution of fundamental shapes, and that the 'shape function/class function' methodology can be used to describe the fundamental shapes as well as the distributions of the fundamental shapes. A number of applications of the 'CST' method to nacelles, ducts, wings and bodies were presented to illustrate the versatility of this new methodology. In this paper, the CST method is extended to include geometric warping such as variable camber, simple flap, aeroelastic and flutter deflections. The use of the CST method for geometric morphing of one geometric shape into another is also shown. The use of CST analytic wings in design optimisation will also be discussed.

NOMENCLATURE

A_i	'*i*th' scaling co-efficient
b	wing span
Bu, Bl	upper and lower wing surface scaling factor
BPO, BPON	Order of the Bernstein polynomial where N = some number
C, c	chord length
CDW	wave drag coefficient
C_{LOCAL}	local chord
$C_{N2}^{N1}(\psi)$	class function value at y (defined by Eq. 6)
C_d	distribution class function
C_s	cross section class function (defined by Equation (22))
CST	class function shape function transformation
e	width to height ratio
H	body height

Paper No. 3281. Manuscript received 23 January 2008, revised version received 31 August 2008, accepted 15 September 2009.

i	variable counter, variable exponent
$K_{r,n}$	binomial coefficient (defined by Equation (9))
Kx_i	streamwise binomial coefficient (defined by Equation (30)
Ky_i	spanwise binomial coefficient (defined by Equation (34))
L	overall length
L.E., *LE*	leading edge
MHB	cross-section maximum half breadth
N, n	number of terms in a summation, order of the Bernstein polynomial
$N1$, $N2$	class function exponents
Nu, Nl	upper and lower surface cross-section class function exponents
NC, $Nc1$, $Nc2$	cross-section class function exponents
$Nd1$, $Nd2$	distriction class function exponents
r	summation counter
RL_E	leading-edge radius
$S(\psi)$	shape function value at ψ(defined by Equation (2)).
$S_{r,n}(\psi)$	Bernstein polynomial term (defined by Equation (8)).
$S_u(\psi)$	upper surface shape function
$S_l(\psi)$	lower surface shape function
$Sx_i(\psi)$	streamwise unit shape function (defined by Equation (29))
$Sy_i(\psi)$	spanwise unit shape function (defined by Equation (33))
T.E., TE	trailing edge
W	body width
y	spanwise co-ordinate
z	vertical co-ordinate
z_{MAX}	Maximum value of z
2D	two-dimensional
3D	three-dimensional
β	trailing-edge boat-tail angle
δ	flap deflection angle
ε	cross section width to height ratio
Δz_{TE}	aerofoil trailing-edge thickness
ψ	non-dimensional chordwise co-ordinate, x/c
η	non-dimensional spanwise co-ordinate, $2y/b$
ζ	non-dimensional vertical co-ordinate, z/c
ζ_T	non-dimensional trailing edge thickness, $\Delta z_{TE}/c$
ζ_L	non-dimensional lower surface co-ordinate, z_L/c
ζ_U	non-dimensional upper surface co-ordinate, z_U/c
ζ_N	non-dimensional local wing shear
$\Delta\alpha_T$	Local wing twist angle

1.0 INTRODUCTION

The choice of the mathematical representations of the geometry of an aircraft or aircraft component, that is utilised in any particular aerodynamic design or multidisciplinary design optimisation process, along with the selection of the type of optimisation algorithm have a profound effect on such things as the computational time and resources, the extent and general nature of the design space which determines whether or not the geometries contained in the design space are smooth or irregular, or even physically realistic or acceptable.

The method of geometry representation also affects the suitability of the selected optimisation process. For example the use of discrete co-ordinates as design variables may not be suitable for use with a genetic optimisation process since the resulting design space could be heavily populated with aerofoils having bumpy irregular surfaces, thus making the possibility of locating an optimum smooth practically impossible. The geometry representation method may also affect whether a meaningful 'optimum' is contained in the design space and if an optimum design exists, whether or not it can be found.

Desirable characteristics for any geometric representation technique include:

- well behaved and produces smooth and realistic shapes
- mathematically efficient and numerically stable process that is fast, accurate and consistent
- requires relatively few variables to represent a large enough design space to contain optimum aerodynamic shapes for a variety of design conditions and constraints
- allows specification of design parameters such as leading-edge radius, boat-tail angle, aerofoil closure.
- provides easy control for designing and editing the shape of a curve
- intuitive – geometry algorithm should have an intuitive and geometric interpretation.

The geometric definition of any aircraft consists of representing the basic defining components of the configuration by utilising two fundamental types of shapes[3] together with the distribution of the shapes along each of the components.

The two fundamental defining shapes include:

Class 1: Wing aerofoil type shapes for defining such components as:

- aerofoils/wings
- helicopter rotors, turbomachinery blades
- horizontal and vertical tails, canards, winglets, struts
- bodies or nacelles of revolution

Class 2: Body cross-section type shapes for defining such components as:

- aircraft fuselages (cross sections)
- rotor hubs and shrouds
- channels, ducts and tubing
- lifting bodies

The mathematical description of Class 1 geometries having a round nose and pointed aft-end is a continuous but non-analytic function because of the infinite slope at the nose and the corresponding large variations of curvature over the surface. Similarly, in the conventional Cartesian coordinate system, the mathematical definitions of the cross-sections of Class 2 type of geometries generally are also continuous but non-analytic functions.

Consequently, a large number of co-ordinates are typically required to describe either Class 1 or Class 2 types of geometries. Numerous methods[4-10] have been devised to numerically represent class 1 aerofoil type geometries for use in use in aerodynamic design, optimisation and parametric studies. Commonly used geometry representation methods typically fail to meet the complete set of the previously defined desirable features[1].

A previous paper[1] focused on the Class 1 type of 2D aerofoil shapes that have a round nose and a pointed aft-end. A new and powerful methodology for describing such geometries was presented. In a subsequent paper[2], the methodology was extended to represent class 2 geometries as well as to general 3D geometries. In the current paper results of the extension of the CST method to more general wing/body geometries will be presented along with initial aerodynamic optimisation results using the CST methodology.

A brief description and review of the methodology presented in the previous papers will be shown since knowledge of this information is essential to the understanding of the extension of the methodology that is presented in the present paper.

The concept of representing arbitrary 3D geometries as distribution of fundamental shapes is discussed. It is shown that the previously method developed for 2D aerofoils and axi-symmetric bodies or nacelles, can be used to mathematically describe both the fundamental shapes as well as the distribution of the shapes for rather arbitrary 3D geometries. Applications of the extended methodology to a variety of 3D geometries including wings and nacelles are shown.

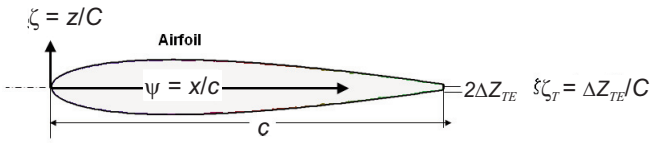

Figure 1. Typical wing aerofoil section.

2.0 ROUND NOSE AEROFOIL REPRESENTATION

A typical subsonic wing aerofoil section is shown in Figure 1. Round nose aerofoils such as shown in the figure, have an infinite slope and an infinite 2nd derivative at the leading edge and large variations in curvature over the aerofoil surface. The mathematical description of an aerofoil must therefore deal with a rather complex non-analytic function over the surface of the aerofoil. Consequently a large number of '*x,z*' co-ordinates are typically required along with a careful choice of interpolation techniques in order to provide a mathematical or numerical description of the surfaces of an aerofoil.

The choice of the mathematical representation of an aerofoil, that is utilised in any particular aerodynamic design optimisation process, along with the selection of the type of optimisation algorithm have a profound effect on such things as:

- Computational time and resources
- The extent and general nature of the design space that determines whether or not the geometries contained in the design space are smooth or irregular, or even physically realistic or acceptable
- If a meaningful 'optimum' is even contained in the design space
- If optimum designs exist, whether or not they can they be found.

The method of geometry representation also affects the suitability of the selected optimisation process. For example the use of discrete coordinates as design variables may not be suitable for use with a genetic optimisation process since the resulting design space could be heavily populated with aerofoils having bumpy irregular surfaces, thus making the possibility of locating an optimum smooth practically impossible.

Desirable design features for any geometric representation technique include:

- Well behaved and produces smooth and realistic shapes
- Mathematically efficient and numerically stable process that is fast, accurate and consistent
- Flexibility
  - Requires relatively few variables to represent a large enough design space to contain optimum aerodynamic shapes for a variety of design conditions and constraints
  - Allows specification of key design parameters such as leading edge radius, boat-tail angle, aerofoil closure.
  - Provide easy control for designing and editing the shape of a curve
- Intuitive – geometry algorithm should have an intuitive and geometric interpretation.
- Systematic and consistent – the way of representing, creating and editing different types of curves (e.g., lines, conic sections and cubic curves) must be the same.
- Robust – the represented curve will not change its geometry under geometric transformations such as translation, rotation and affine transformations.

Commonly used geometry representation methods typically fail to meet the complete set of desirable features[1].

3.0 MATHEMATICAL DESCRIPTION OF AEROFOIL GEOMETRY

In the case of the round nose aerofoil described in a fixed Cartesian co-ordinate system, the slopes and 2nd derivatives of the surface geometry are infinite at the nose and large changes in curvature occur over the entire aerofoil surface. The mathematically characteristics of the aerofoil surfaces are therefore non-analytic function with singularities in all derivatives at the nose. The approach used in Ref. 1 to develop an improved aerofoil geometry representation method is based on a technique that the author has often used successfully in the past, to develop effective computational methods to deal with numerically difficult functions.

The technique included the following steps:

1. Develop a general mathematical equation necessary and sufficient to describe the geometry of any round nose/sharp aft end aerofoil;
2. Examine the general nature of this mathematical expression to determine the elements of the mathematical expression that are the source of the numerical singularity
3. Rearrange or transform the elements of the mathematical expression to eliminate the numerical singularity.
4. This resulted in identifying and defining a 'shape function' transformation technique such that the 'design space' of an aerofoil utilising this shape function becomes a simple well behaved analytic function with easily controlled key physical design features in addition to possessing an inherent strong smoothing capability.
5. Subsequently a 'Class Function' was introduced to generalise the methodology for applications to a wide variety of fundamental 2D aerofoils and axi-symmetric nacelle and body geometries.

A summary of this approach is discussed below.

The general and necessary form of the mathematical expression that represents the typical aerofoil geometry shown in Fig. 1 is:

$$\zeta(\psi) = \sqrt{\psi}(1-\psi)\sum_{i=0}^{N} A_i \psi^i + \psi\zeta_T \qquad \ldots (1)$$

Where: $\psi = x/c$ $\zeta = z/c$ and $\zeta_T = \Delta\zeta_{TE}/c$.

The term $\sqrt{\psi}$ is the only mathematical function that will provide a round nose.

The term $(1 - \psi)$ is required to insure a sharp trailing-edge.

The term $(\psi\, \zeta_T)$ provides control of the trailing edge thickness.

The term $A_i\psi^i$ represents a general function that describes the unique shape of the geometry between the round nose and the sharp aft end. This term is shown for convenience as a power series but it can be represented by any appropriate well behaved analytic mathematical function.

4.0 AEROFOIL SHAPE FUNCTION

The source of the non-analytic characteristic of the basic aerofoil equation is associated with the square root term in Equation (1).

Let us define the shape function 'S(ψ)' that is derived from the basic geometry equation by first subtracting the base area term and then dividing by the round nose and sharp end terms.

This gives:

$$S(\psi) \equiv \frac{\zeta(\psi) - \psi\zeta_T}{\sqrt{\psi}\bullet[1-\psi]} \qquad \ldots (2)$$

The equation that represents the 'S' function which is obtained from Equations 1 and 2 becomes the rather simple expression:

$$S\left(x/L\right) = \sum_{i=0}^{N}\left[A_i \bullet \left[\frac{x}{L}\right]^i \right] \quad \ldots(3)$$

The 'shape function' equation is a simple well behaved analytic equation for which the 'eye' is well adopted to see the represented detailed features of an aerofoil and to make critical comparisons between various geometries.

It was shown in Ref. 1, that the nose radius, the trailing edge thickness and the boat-tail angle are directly related to the unique bounding values of the 'S(ψ)' function.

The value of the shape function at $x/c = 0$ is directly related to the aerofoil leading-edge nose radius by the relation:

$$S(0) = \sqrt{2\,R_{LE}/C} \quad \ldots(4)$$

The value of the shape function at $x/c = 1$ is directly related to the aerofoil boat-tail angle, β, and trailing edge thickness, ΔZte, by the relation:

$$S(1) = \mathrm{Tan}\,\beta + \zeta_T \quad \ldots(5)$$

Hence, in the transformed coordinate system, specifying the endpoints of the 'S' function provide an easy way to define and to control the leading edge radius, the closure boat-tail angle and trailing edge thickness.

An example of the transformation of the actual aerofoil geometry to the corresponding shape function is shown in Fig. 2. The transformation of the constant *Zmax* height line, and the constant boat-tail angle line, are also shown in the transformed plane.

The shape function for this example aerofoil is seen to be approximately a straight line with the value at zero related to the leading edge radius of curvature and the value at the aft end equal to tangent of the boat-tail angle plus the ratio of trailing-edge thickness/chord length. It is readily apparent that the shape function is indeed a very simple analytic function.

The areas of the aerofoil that affects its drag and performance characteristics of the aerofoil are readily visible on the shape function curve as shown in the figure. Furthermore, the shape function provides easy control of the aerofoil critical design parameters.

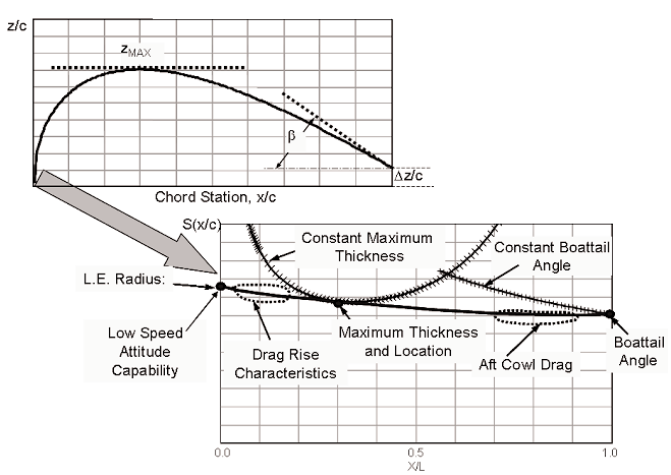

Figure 2. Example of an aerofoil geometric transformation.

The term $\sqrt{\psi}[1-\psi]$ will be called the 'Class Function' C(ψ) With the general form

$$C_{N2}^{N1}(\psi) = (\psi)^{N1}\left[1-\psi\right]^{N2} \quad \ldots(6)$$

For a round nose aerofoil N1 = 0·5 and N2 = 1·0

In Reference 1, it was shown that different combinations of the exponents in the class function define a variety of basic general classes of geometric shapes:

N1 = 0·5 and N2 = 1·0 define a NACA type round nose and pointed aft end aerofoil.

N1 = 0·5 and N2 = 0·5 define an elliptic aerofoil, or an ellipsoid

N1 = 1·0 and N2 = 1·0 define a biconvex aerofoil, or an ogive body.

N1 = 0·75 and N2 = 0·75 define the radius distribution of a Sears-Haack body

N1 = 0·75 and N2 = 0·25 define a low drag projectile

N1 = 1·0 and N2 = 0·001 define a cone or wedge aerofoil.

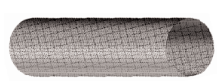

N1 = 0·001 and N2 = 0·001 define a rectangle, or circular rod.

The 'class function' is used to define general classes of geometries, whereas the 'shape function' is used to define specific shapes within the geometry class.

Defining an aerofoil shape function and specifying it's class function is equivalent to defining the actual aerofoil coordinates which are obtained from the shape function and class function as:

$$\zeta(\psi) = C_{N2}^{N1}(\psi) \bullet S(\psi) + \psi \bullet \zeta_T \quad \ldots(7)$$

5.0 REPRESENTING THE SHAPE FUNCTION

A number of different techniques of representing the shape function for describing various geometries will be described in this report. The simplest approach is illustrated in Fig. 3. The figure shows the fundamental baseline aerofoil geometry derived from the simplest of all shape functions, the unit shape function: $S(\psi) = 1$. Simple variations of the baseline aerofoil are also shown with individual parametric changes of the leading edge radius, and of the location of maximum thickness.

The figure on the left shows changes in the leading edge radius and the front portion of the aerofoil obtained by varying the value of $S(0)$ with a quadratic equation that is tangent to the *Zmax* curve at *x/c* for *Zmax*. The maximum thickness, maximum thickness location and boat-tail angle remained constant.

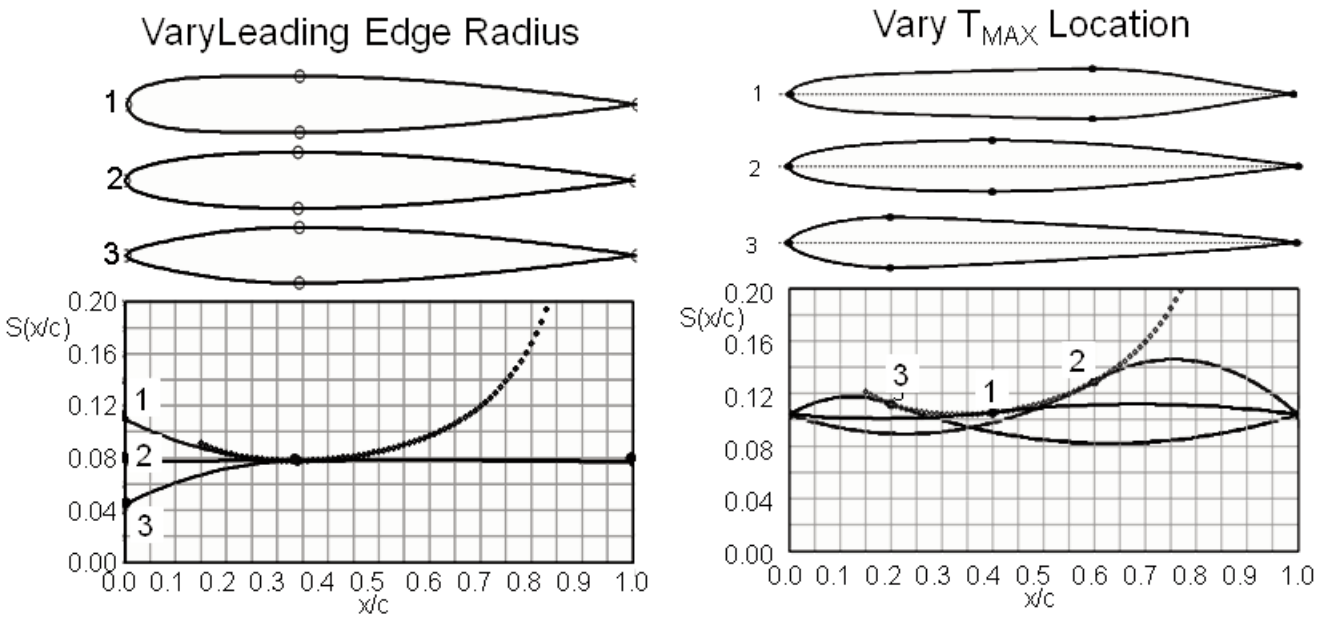

Figure 3. Examples of one variable aerofoil variations.

The figure on the right shows the effect varying the location of maximum thickness while keeping the values of the maximum thickness, the nose radius and the aft boattail angle of the aerofoil unchanged. In each of these examples the aerofoil shape changes are controlled by a single variable and in all cases the resulting aerofoil is both smooth and continuous

Figure 4 shows a five variable definition of a symmetric $C_{1\cdot0}^{0\cdot5}(\psi)$ aerofoil using the shape function. The corresponding aerofoil geometry is also shown. The variables include:

1. Leading-edge radius
2. Maximum thickness
3. Location of maximum thickness
4. Boattail angle
5. Closure thickness

A cambered aerofoil can be defined by applying the same technique to both the upper and the lower surfaces. In this instance the magnitude of the value of the shape function at the nose, $S(0)$, of the upper surface is equal to that on the lower surface. This insures that the leading edge radius is continuous from the upper to the lower surface of the aerofoil. The value of the half thickness at the trailing edge is also equal for both surfaces. Consequently, as shown in Fig. 5, eight variables would be required to define the aforementioned set of parameters for a cambered aerofoil.

In the examples shown in Figs 4 and 5, the key defining parameters for the aerofoils are all easily controllable with the shape function.

6.0 AEROFOIL DECOMPOSITION INTO COMPONENT SHAPES

The unit shape function can be decomposed into scalable component aerofoils[1] by representing the shape function with a Bernstein polynomial of order 'N' as shown in Fig. 6.

The representation of the unit shape function in terms of increasing orders of the Bernstein polynomials provides a systematic decomposition of the unit shape function into scaleable components. This is the direct result of the 'partition of unity' property which

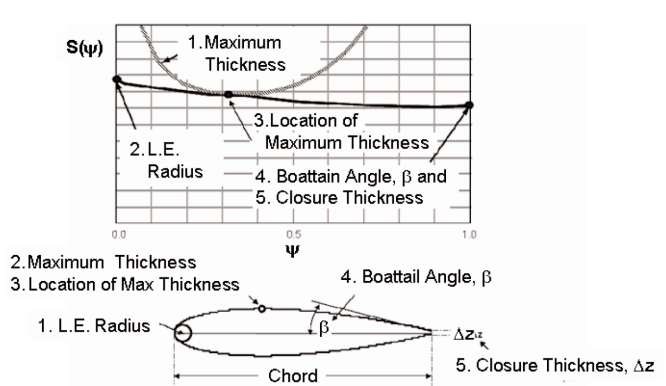

Figure 4. Symmetric aerofoil five variables definition.

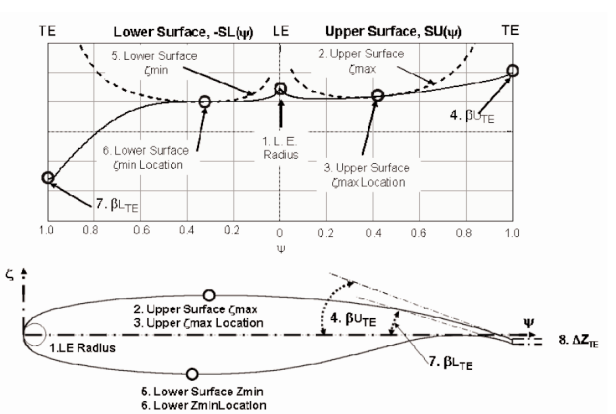

Figure 5. Cambered aerofoil eight variables definition.

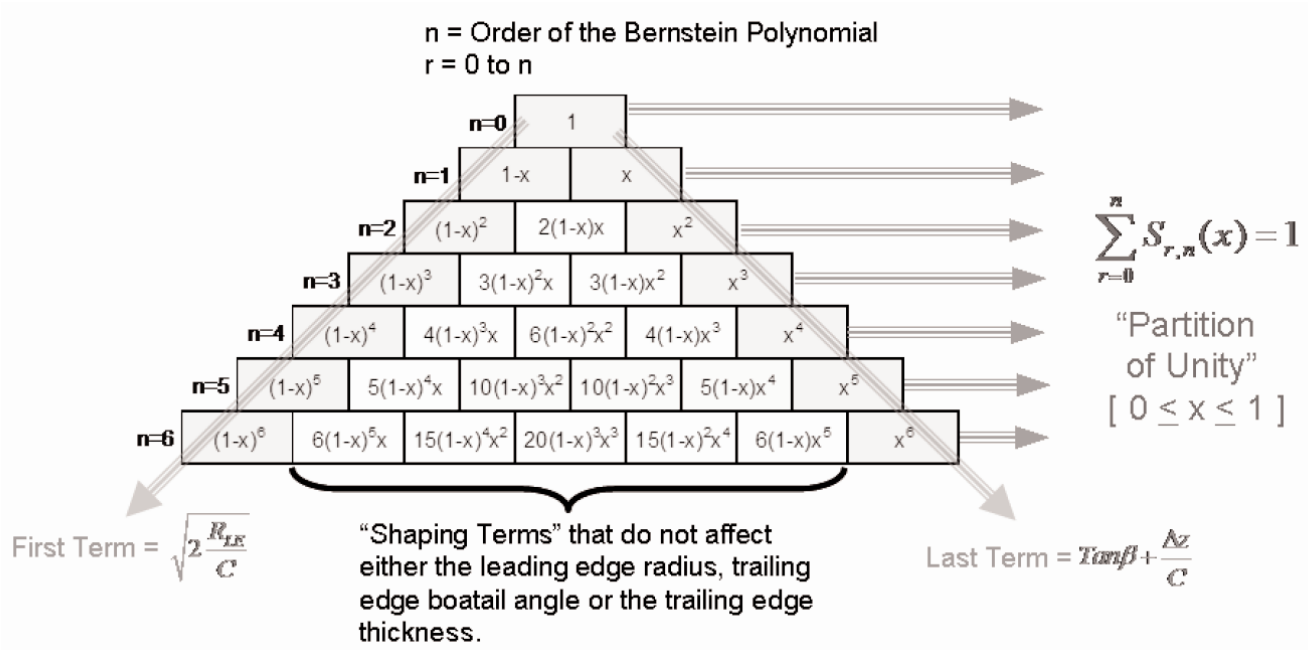

Figure 6. Bernstein polynomial decomposition of the unit shape function.

states that the sum of the terms, which make up a Bernstein polynomial of any order, over the interval of 0 to 1, is equal to one. This means that every Bernstein polynomial represents the unit shape function. Consequently, the individual terms in the polynomial can be scaled to define an extensive variety of aerofoil geometries[1].

The Bernstein polynomial of any order 'n' is composed of the "n+1" terms of the form:

$$S_{r,n}(x) = K_{r,n} x^r (1-x)^{n-r} \quad \ldots (8)$$

r = 0 to n
n = order of the Bernstein polynomial

In the above equation, the coefficients factors $K_{r,n}$ are binominal coefficients defined as:

$$K_{r,n} \equiv \binom{n}{r} \equiv \frac{n!}{r!(n-r)!} \quad \ldots (9)$$

For any order of Bernstein polynomial selected to represent the unit shape function, only the first term defines the leading-edge radius and only the last term defines the boat-tail angle. The other in-between terms are 'shaping terms' that neither affect the leading edge radius nor the trailing-edge boat-tail angle.

Examples of decompositions of the unit shape function using various orders of Bernstein polynomials are shown in Fig. 7 along with the corresponding component aerofoils.

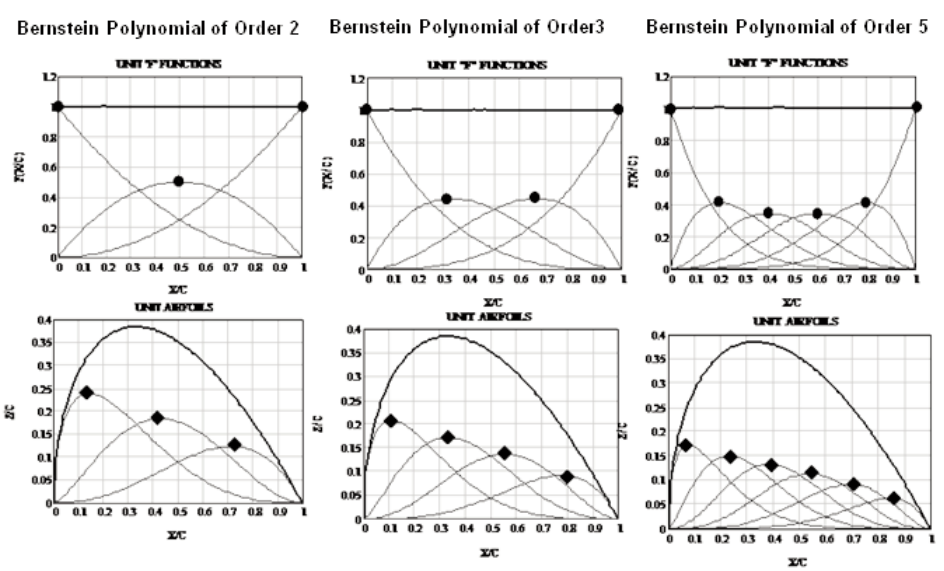

Figure 7. Bernstein polynomial provides 'natural shapes'.

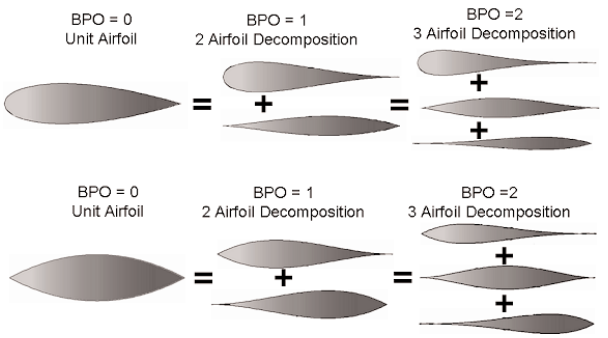

Figure 8. Example component aerofoils.

The locations of the peaks of the component 'S' functions are equally spaced along the chord as defined by the equation:

$$(\psi)_{S\max i} = \frac{i}{n} \qquad \text{for } i = 0 \text{ to } n \qquad \ldots (10)$$

The corresponding locations of the peaks of the component aerofoils are also equally spaced along the chord of the aerofoil and are defined in terms of the class function exponents and the order of the Bernstein polynomial by the equation:

$$(\psi)_{Z\max} = \frac{N1+i}{N1+N2+n} \qquad \text{for } i = 0 \text{ to } n \qquad \ldots (11)$$

The technique of using Bernstein polynomials to represent the shape function of an aerofoil in reality defines a systematic set of component aerofoil shapes that can be scaled to represent a variety of aerofoil geometries as shown in Fig. 8.

7.0 AEROFOILS DEFINED USING BERNSTEIN POLYNOMIALS REPRESENTATION OF THE UNIT SHAPE FUNCTION

The upper and lower surfaces of a cambered aerofoil, can each be defined using Bernstein polynomials of any selected order n, to describe a set of component shape functions that are scaled by 'to be determined' coefficients as shown in the following equations.

The component shape functions are defined as:

$$S_i(\psi) = K_i \psi^i (1-\psi)^{n-i} \qquad \ldots (12)$$

Where the term K_i is the binomial co-efficient which is defined as:

$$K_i \equiv \binom{n}{i} = \frac{n!}{i!(n-i)!} \qquad \ldots (13)$$

Let the trailing-edge thickness ratios for the upper and lower surface of an aerofoil be defined as:

$$\Delta\zeta_U = \frac{zu_{TE}}{C} \quad \text{and} \quad \Delta\zeta_L = \frac{zl_{TE}}{C} \qquad \ldots (14)$$

The class function for the aerofoil is:

$$C_{N2}^{N1}(\psi) = \psi^{N1} \bullet (1-\psi)^{N2} \qquad \ldots (15)$$

The overall shape function equation for the upper surface is:

$$Su(\psi) = \sum_{i=1}^{n} Au_i \bullet S_i(\psi) \qquad \ldots (16)$$

The upper surface defining equation is:

$$\zeta_U(\psi) = C_{N2}^{N1}(\psi) \bullet Su(\psi) + \psi \bullet \Delta\zeta_U \qquad \ldots (17)$$

The lower surface is similarly defined by the equations:

$$Sl(\psi) = \sum_{i=1}^{n} Al_i \bullet S_i(\psi) \qquad \ldots (18)$$

and

$$\zeta_L(\psi) = C_{N2}^{N1}(\psi) \bullet Sl(\psi) + \psi \bullet \Delta\zeta_L \qquad \ldots (19)$$

The coefficients Au_i and Al_i can be determined by a variety of techniques depending on the objective of the particular study. Some examples include:

- Variables in a numerical design optimisation application
- Least squares fit to match a specified geometry
- Parametric shape variations.

The method of utilising Bernstein polynomials to represent an aerofoil has the following unique and very powerful properties[1]:

- This aerofoil representation technique, captures the entire design space of smooth aerofoils
- Every aerofoil in the entire design space can be derived from the unit shape function aerofoil
- Every aerofoil in the design space is therefore derivable from every other aerofoil

8.0 AEROFOIL REPRESENTATION ➔ KEY CONVERGENCE QUESTION

A key convergence question relative to the class function/shape function geometry method for defining aerofoils, nacelles or bodies of revolution is the following. What orders of Bernstein polynomials, BPO, are required to capture enough of a meaningful design space to contain a true optimum design?

A two step approach was defined in order to obtain the answer for this question:

1) Compare actual aerofoil and represented aerofoil geometries for a wide variety of aerofoils

- Use various orders of Bernstein polynomials for the shape function to approximate the actual aerofoils shape functions computed from the defined aerofoil co-ordinates. The coefficients for the component Bernstein polynomial shape functions were to be determined by least squares fits to the selected

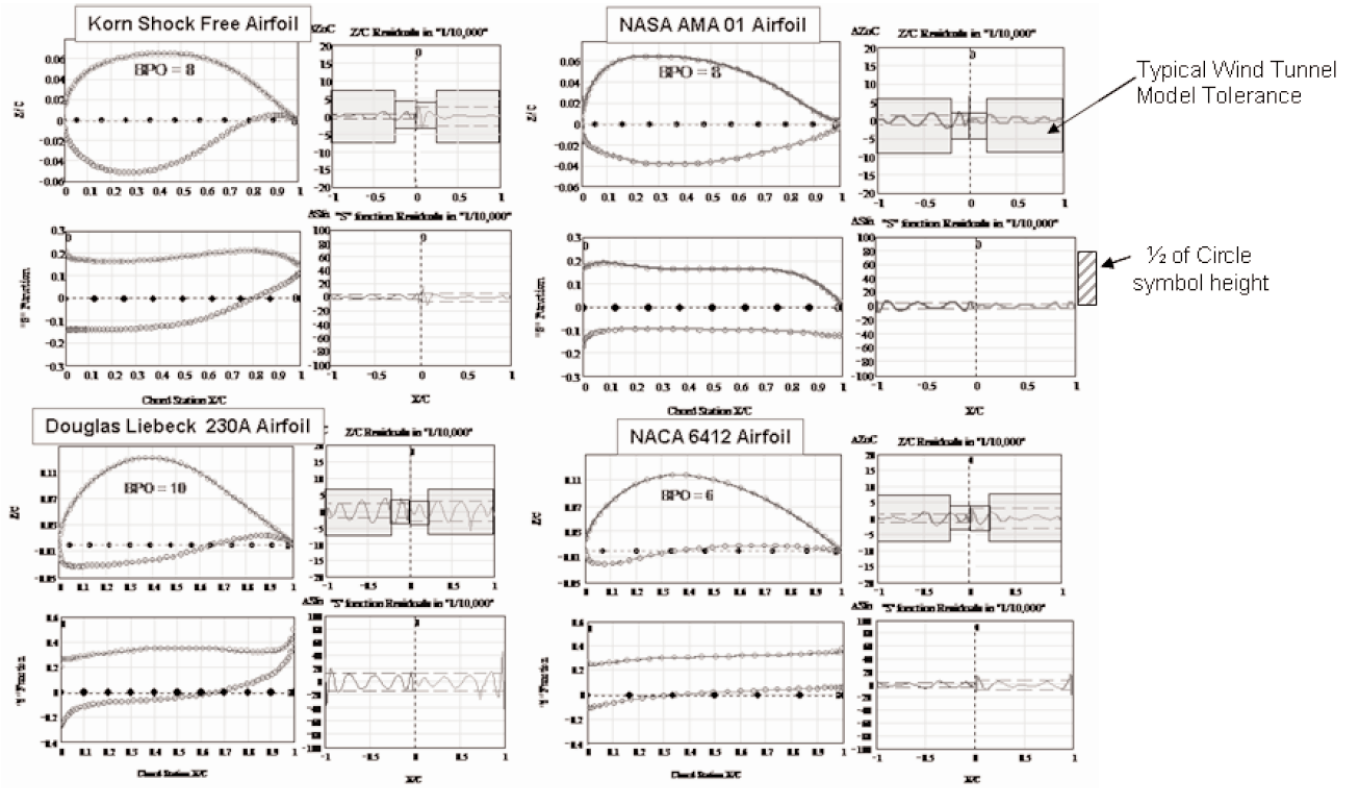

Figure 9. Typical CST aerofoil representations.

aerofoil upper and lower surface shape functions. For all study aerofoils, approximate aerofoils were determined for Bernstein polynomial representation of the shape functions of orders 2 to 15/

- Investigate a wide variety of optimum and non-optimum, symmetric and cambered aerofoil geometries.
- Compute the statistical measures such as 'residual differences', 'standard deviations' and 'correlation functions' to quantify the 'mathematical goodness' of the representations for each of the study aerofoils.
- Compare surface slopes, 2nd derivatives and curvature between actual and approximate aerofoil shapes

2) Conduct TRANAIR[11,12] with boundary layer CFD analyses of the actual and the corresponding shape function defined aerofoils for a range of Mach numbers and angle of attacks.

- Compare upper and lower surface pressure distributions between those obtained with the actual and approximate geometries.
- Compare lift, drag and pitching moment characteristics between the actual and approximate aerofoils

More than 30 aerofoils have been analysed applying this process. These include symmetric NACA aerofoils, cambered NACA aerofoils, high lift aerofoils, natural laminar flow aerofoils, shock-free aerofoils, supercritical aerofoils and transonic multipoint optimised aerofoils. For each of the study aerofoils, approximate aerofoil geometries were defined using Bernstein polynomial surface representations of the upper and lower surfaces shape functions, of orders 2 to 15, to critically evaluate the geometry convergence characteristics. Results of these extensive investigations were reported in Ref. 1.

Typical examples of shape function representation of a variety of aerofoils are shown in Fig 9.

The defining aerofoil co-ordinates are shown by the circles. The approximating geometries are shown as the lines through the points. Bands corresponding to typical wind-tunnel tolerances are shown in the co-ordinate residual curves. Bars corresponding to ½ of the height of the circular symbols representing the actual aerofoil geometry, are indicated on the figures.

The results of the previously reported extensive[1] assessments of the adequacy of the shape function methodology utilising Bernstein polynomials to represent a wide variety of aerofoils, showed that a relatively low order Bernstein polynomial, (typically BPO6 to BPO9), matched the aerofoils geometries, slopes and 2nd derivatives as well as the pressure distributions and aerodynamic forces[1]. The results also indicated that lower order Bernstein polynomials, corresponding to fewer design variables, (perhaps BPO4 to BPO6), should be adequate for developing optimum designs.

The CST methodology offers the option for a systematic approach for design optimisation. The optimisation process can initially be conducted with a family of component aerofoil shapes corresponding to a low order BP representation for the shape function to obtain an optimum design. The order of the BP can then be increased to conduct another optimisation to determine if a better optimum design is achieved. Increasing the order of the BP is a systematic way to increase the number of design variables and thereby explore the convergence to an optimum solution.

9.0 GEOMETRY WARPING AND MORPHING

The CST methodology can be readily adapted to describe both warping and morphing of geometric components. We will define 'warping' to mean a continuous family of transformations of a graphical object. Warping retains the fundamental characteristics of the initial object. Examples of warping include:

- Wing twist
- Simple flap deflection: transformation with fixed topology
- Aeroelastic static deflections
- Flutter dynamic deflections

We define 'morphing' (metamorphosis) to mean transformations between graphical objects. Morphing involves variation of the fundamental characteristics of the initial object to those of the target object. Examples of morphing include:

- Parametric leading-edge radius variation (Fig 3)
- Parametric change in the location of maximum thickness of an aerofoil (Fig. 3)
- A fuselage can be considered a morphing of cross section shapes along the length of the body

It will be shown further in this report that geometric morphing can be easily obtained by variations of class function/shape function variables. Warping involves geometric variations external to the class function/shape function variables.

Figure 10 shows examples of geometric warping. These were obtained by defining the forward and aft pivot points. The chord lines forward of the front pivot point and aft of the back pivot point are deflected according to a prescribed deflection shape. The simple flap has a discontinuous linear rotation. The variable camber is obtained with a cubic equation. Both type of deflections have two variables that include the pivot point location and the shape exponent of the deflection curve. The physical length of the deflected chord is retained. The original upper and lower surface local heights normal to the chord length are retained along the deflected chords.

The aeroelastic deflections were obtained in a similiar manner.

The discussions so far have been focused in 2D round nose/sharp aft-end aerofoils. However, as shown in Fig. 11, different combinations of the exponents in the class function defines a variety of basic general classes of geometric shapes of aerofoils, bodies of revolution and axi-symmetric nacelles. The use of the class function therefore, allows the previously discussed shape function methodology as well as the studies conclusions to apply equally well to a wide variety of 2D and axi-symmetric geometries.

10.0 EXTENSION TO ARBITRARY 3D GEOMETRIES

The shape functions/class function methodology can be used to describe both the upper and the lower lobes of a body cross-section similar to the upper and lower surface of an aerofoil. Let us initially assume that a body cross-section is laterally symmetric and has the shape of an ellipse as shown in the Fig 12. We will then subsequently generalise the results using the class function.

The equation for the ellipse with the axes of the ellipse at the left edge can be expressed as:

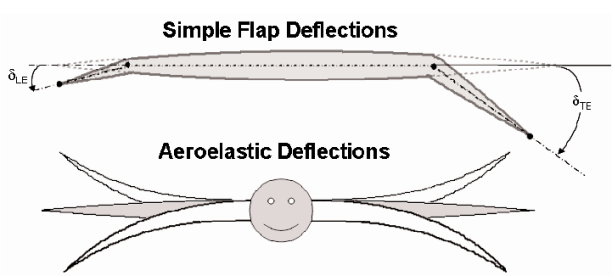

Figure 10. Examples of geometric warping.

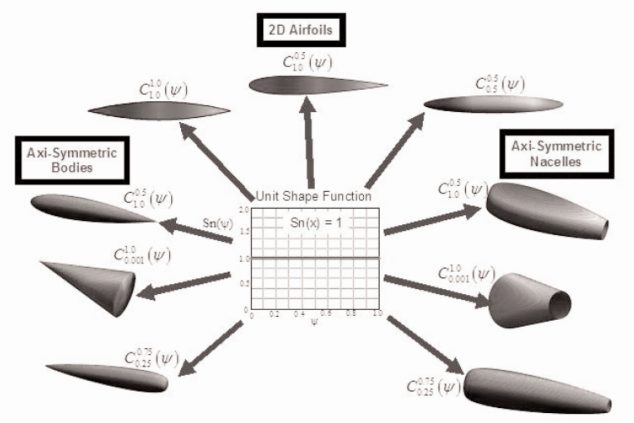

Figure 11. Geometries derivable from a unit shape function.

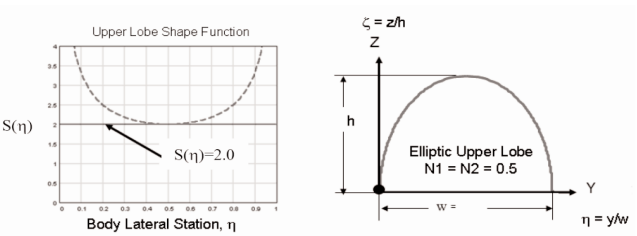

Figure 12. Representation of a body upper or lower lobe shape.

$$\zeta(\eta) = 2\eta^{0.5}(1-\eta)^{0.5} \qquad \ldots (20)$$

Where: $\eta = y/w$ and $\zeta = z/h$

The shape function for this upper lobe elliptic geometry is therefore:

$$Su(\eta) = \frac{\zeta u(\eta)}{\eta^{NC1}(1-\eta)^{NC2}} = 2 \qquad \ldots (21)$$

In the above equation we have generalised the expression by using the arbitrary exponents NC1 and NC2

$$Cs(\eta) = \eta^{NC1}(1-\eta)^{NC2} \qquad \ldots (22)$$

$Cs(\eta)$ will be called the cross-section class function.

In this case the upper lobe defining equation is:

$$\zeta u(\eta) = \left[Su(\eta) \equiv 2 \right] Cs^{0.5}_{0.5}(\eta) \qquad \ldots (23)$$

For an elliptic upper lobe shape, the shape function is a constant and equal to 2·0, and the class function exponents are: $NC1 = NC2 = 0{\cdot}5$. Figure 13 shows examples of variety of cross-section shapes that can be obtained by independently varying the class function coefficients for the upper and lower lobes of the body cross-section. In these examples, the shape function is a constant value. Any of the geometries can be morphed from the circle by continuously varying the

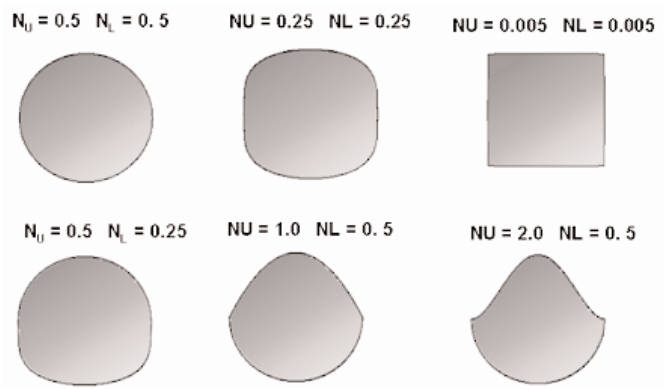

Figure 13. Example upper lobe/lower lobe body cross sections.

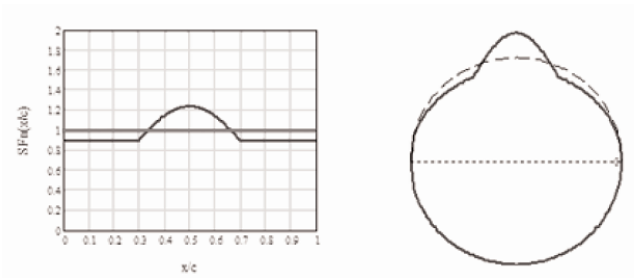

Figure 14. Fuselage 'bump' representation.

class function co-efficients from those of the circle to those of the desired geometric shape. The condition of constant cross-sectional area during the geometric morphing can be easily imposed.

By using the previously described Bernstein polynomial technique to represent the unit shape function together with the body cross-section aspect ratio of the body cross-section (ratio of body cross-section width to body cross-section height), a limitless variety of smooth cross-sectional geometries can be generated with just a few variables.

The example cross-sections shown in Fig. 13 were obtained using simple unit shape functions but different class functions. Very general cross-sectional shapes can be generated by varying the shape function formulations in addition to the class functions. As shown in Fig. 14, changing the shape function for the upper body lobe can create upper surface bumps or fairings. In the examples shown, the geometries are representative of a cross-section of a fuselage through the cockpit area.

Three dimensional bodies in general can be represented as a cross-sectional shape together with a distribution or morphing of the cross-section shape along the length of the body. This is shown in Fig. 15 by the examples of a duct, a high-aspect ratio wing, and a supersonic type integrated wing-body.

The concept of using the shape function/class function methodology to describe both the fundamental cross-sectional shapes and the distribution of the shapes along the body axis is shown for the simple case of a cube in Fig. 16.

The square cross-section can be described by a class function with 'zero exponents', $Cs^{0.005}_{0.005}(\eta)$, and a unit shape function. The longitudinal area distribution controls the distribution of the cross section shapes. The longitudinal area distribution for a cube can be represented by a similar class function, $Ca^{0.005}_{0.005}(\psi)$.

Figure 17 shows a number of relatively simple 3D bodies that can be obtained by various combinations of the cross section and distribution class function exponents. Comparing the third and fourth geometries in the figure, it can be seen that a distribution class

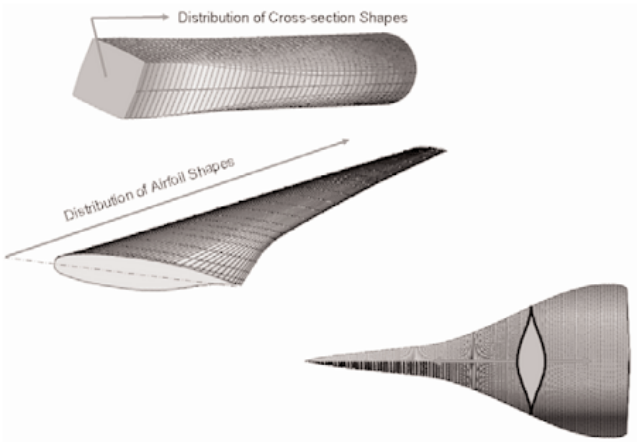

Figure15. Examples of 3D geometries as distribution of shapes.

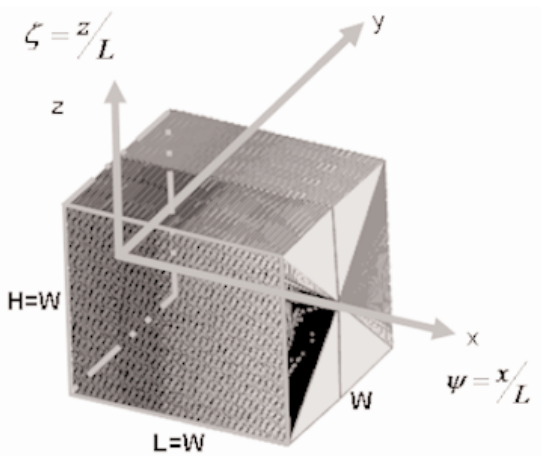

Figure 16. Definitions of cross-section shape and distribution.

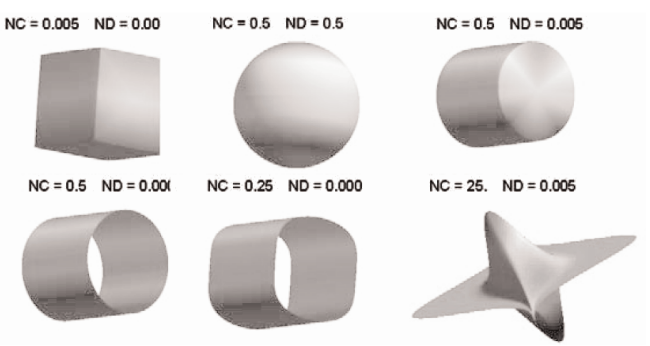

Figure 17. Simple 3D bodies obtained by various cross section and distribution class function exponents.

function exponent slightly greater than zero results in a solid geometry while a distribution class function exactly equal to zero results in a similar but flow through geometry.

Figure 18 shows an example of using the shape function/class function methodology to make an apparently significant geometry change with very few design variables, by morphing a cube into an equal volume Sears-Haack body.

The circular cross-section of the Sears-Haack body has unit shape function and class functions exponents equal to $Cs^{0.5}_{0.5}(\eta)$. The longitudinal radius distribution of a Sears-Haack body has a unit shape

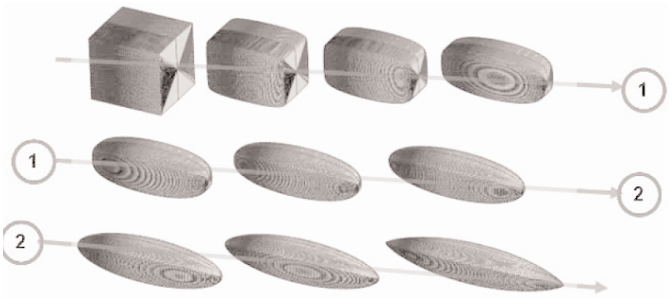

Figure 18. Three variable morphing of a cube into a Sears-Haack body.

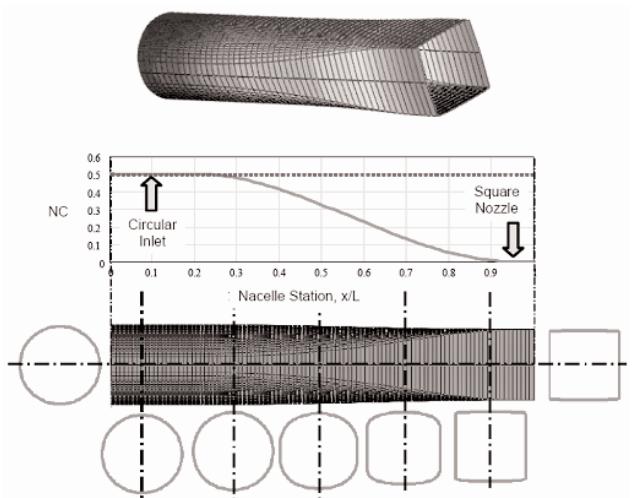

Figure 19. One variable definition of a circular duct with a square nozzle.

function and a class function equal to $Cd^{0.75}_{0.75}(\psi)$

Consequently the morphing of the cube into a Sears-Haack body is easily obtained by simultaneous:

- Increasing the cross-section class function exponents from 0·005 to 0·5
- Increasing the longitudinal radius distribution class function exponents from 0·005 to 0·75
- Increasing the length to keep the volume constant.

An example of morphing a constant area circular duct into a duct with geometry that varies from a circular inlet to a square shaped nozzle 1s shown in Fig. 19. This seemingly complicated geometric transformation was easily defined using as a single variable the class function exponents.

The initial geometry shape at the inlet is a circular duct defined with a cross-section class function with exponents equal to '0·5'. The duct geometry, in this example, retains a constant cross section from 0 to 20% of the length. The last 5% length of the duct has a square cross-section which has class function exponents equal to '0·005'. The width/depth of the square were sized to match the circular inlet area.

In between 20% and 95% of the length, the class function exponents were decreased from 0·5 at 20% to 0·005 at 95% by a cubic variation with zero slopes at both ends. Along the transition region the width and depth were scaled proportionally to keep the cross section area constant. The entire geometry is in reality driven by a single variable, the aft end constant class function exponent

This is an example of a 'scalar' or 'analytic' loft in which the geometry is generated by the analytic variation of the shape defining parameters along the length of the duct.

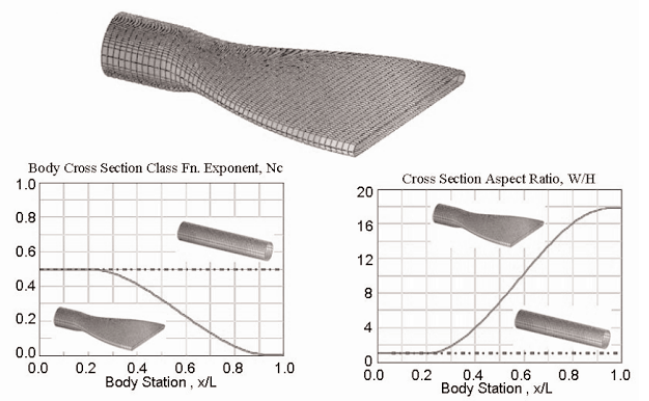

Figure 20. Two variable transformation of a circular duct to a thin rectangular nozzle.

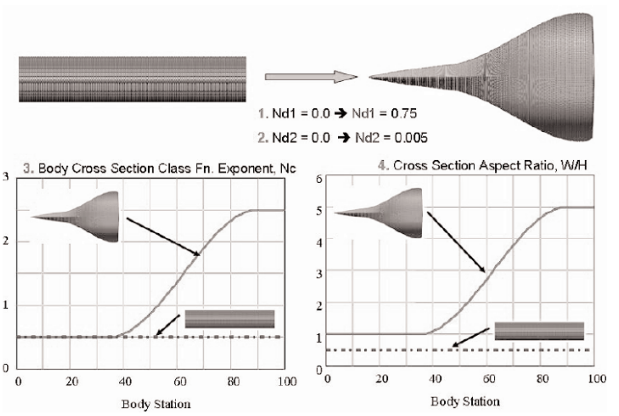

Figure 21. Transformation of a circular cylinder in a 'supersonic transport'.

By adding as an additional variable, the body cross section aspect ratio, the circular duct can be morphed into a duct having a circular inlet and transitions into a wide rectangular nozzle as shown in Fig 20. The body cross-section aspect ratio is defined as the ratio of body width-to-body height.

In Fig. 21, using a similar technique to that used to define the duct in Figs 19 and 20, a flow through circular duct is transformed to a solid geometric shape that appears very similar to a supersonic aircraft configuration.

This geometric transformation was obtained with a total of four design variables. The four design variables included:

- Longitudinal class function exponents: *Nd*1, *Nd*2
- Aft end cross-section class function exponent, *NC*,
- the width-to-height ratio at the aft end: *e*2

11.0 NACELLE DESIGN – 2 OPTIONS

There are two options for using class functions and shape functions for defining a nacelle. These include:

1. Define longitudinal profile shapes for crown line, maximum half-breadth, and keel line and then distributing these profiles circumferentially around the longitudinal axis to define the nacelle geometry.
2. Define cross section shapes and distribute the shapes along the longitudinal axis as controlled by an area distribution.

In the discussions that follow, we will focus on the first option,

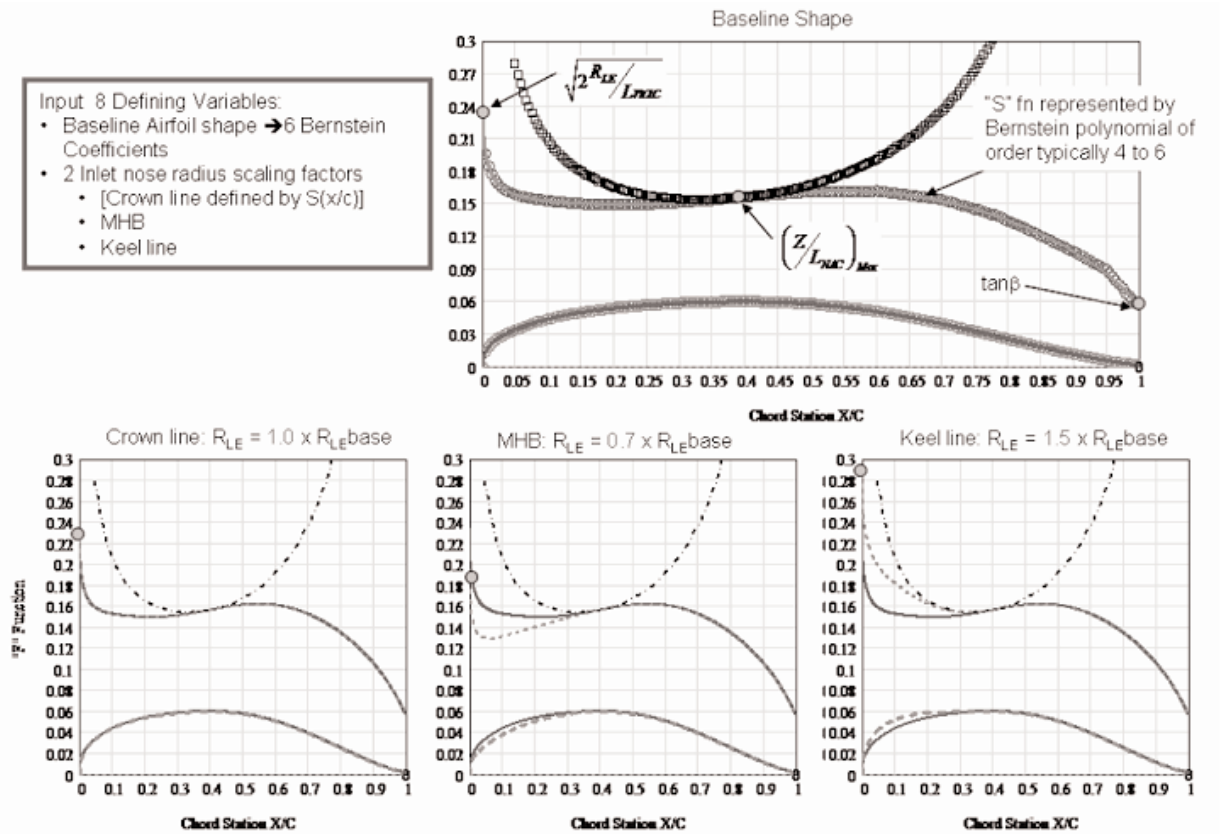

Figure 22. Nacelle crown line, keel line and max half-breadth definitions ~ eight variables.

since this will provide a demonstration of the combined use of many of the concepts that have been discussed in this report and in the previous studies[1,2]. The objective is to develop a detailed nacelle definition with the use of very few design variables.

Figure 22 shows the common approach to defining a nacelle using aerofoil type sections for the crown line, keel line and maximum half breadth shapes. In the example, the basic aerofoil geometry is represented by a BP5 shape function definition for a supercritical type aerofoil which therefore has six defining variables.

The keel line aerofoil and the max half breadth aerofoils in this example are both parametrically modified forward of the maximum thickness station to increase the leading-edge radius in the former case and decrease the leading edge in the latter case. This results in the addition of two more defining variables corresponding to the desired leading edge radii.

The external cross-sectional shape of the nacelle between the crown, max half breadth and keel is defined by an upper lobe class function with the exponent *NU*. The lower lobe of the nacelle is similarly defined by lower lobe class function with the exponent *NL*. This approach to distribute the longitudinal aerofoil shapes circumferentially around the nacelle is shown in Fig. 23. This is achieved by the use of cross-section class functions in which the class function exponents are varied along the length of the nacelle as shown in the figure.

The upper lobe for the entire nacelle is defined using a constant class function exponents of 0·5. This results in an elliptic/circular cross sectional shape distribution between the crown line and the maximum half-breadth aerofoils.

The lower lobe cross-section class function exponents equal 0·25 out to defining station 1 which is located at 40% of the nacelle length. This results in a 'squashed' shape distribution from the maximum half-breadth aerofoil to the keel line aerofoil over the front portion of the nacelle.

The lower lobe aft of defining Station 2, which occurs at 80% of the nacelle length, is circular with a class function exponent equal to 0·5. Consequently this results in an axi-symmetric nozzle geometry.

In between Station 1 and Station 2, the lower lobe shape joining the maximum half-breath geometry and the keel geometry, varies smoothly from a squashed section at station 1 to a circular section at Station 2. The cross-sectional shape distribution is therefore defined entirely by the following four design variables:

- Upper lobe class function exponents, *NU*
- Lower lobe class functions, *NL*
- End of squashed lower lobe station, Station 1
- Start of circular lower lobe station, Station 2

The inlet definition is shown in Fig. 24. The internal inlet cross-section shape and leading edge radii distribution were defined to match the external cowl cross-section shape and streamwise leading edge radius distribution at the nose of the nacelle.

The internal inlet shape morphed smoothly from the 'squashed' shape at inlet lip to a circular cross-section at the throat station. The internal shape was defined as circular aft of the throat station to the end of the inlet length.

The entire internal inlet geometry required only four more defining variables. These include:

- Throat Station
- Throat Area
- End of Inlet Station
- End of Inlet Area

The complete nacelle geometry as defined by the aforementioned 15 total nacelle design variables is shown in Fig. 25. The geometry is seen to be everywhere smooth and continuous.

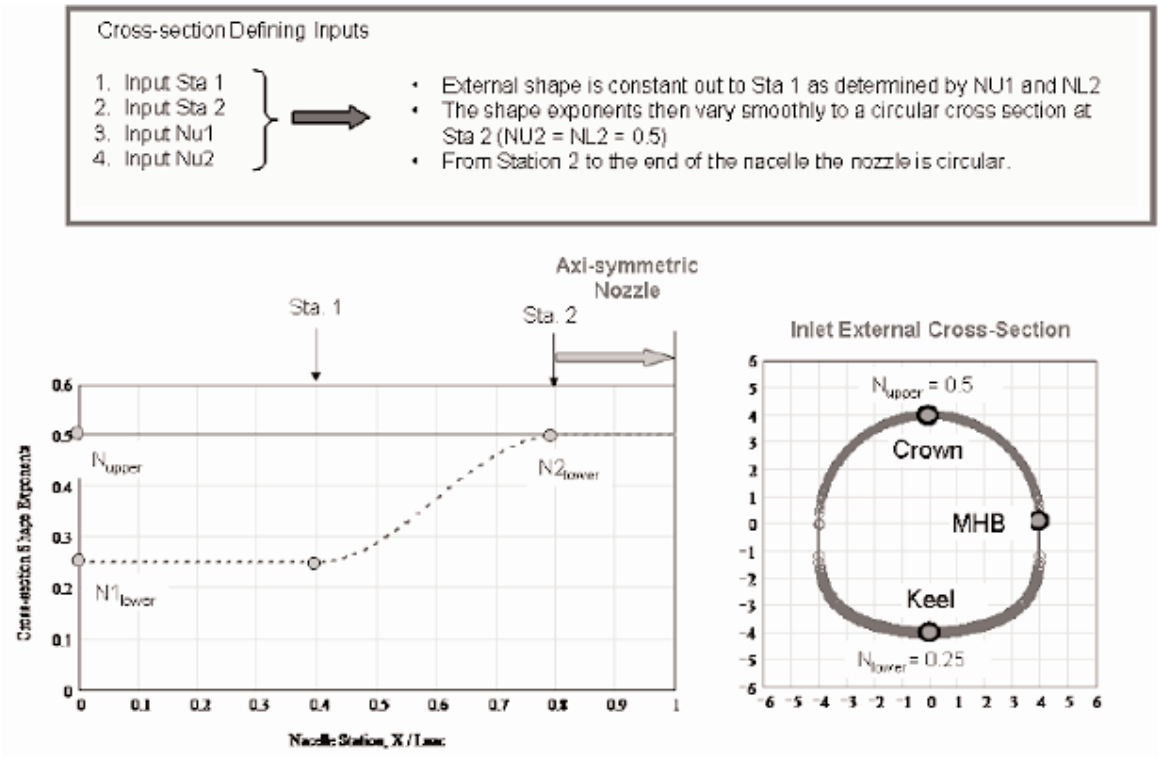

Figure 23. Nacelle shape distribution circumferentially around the nacelle centerline ➔ four variables.

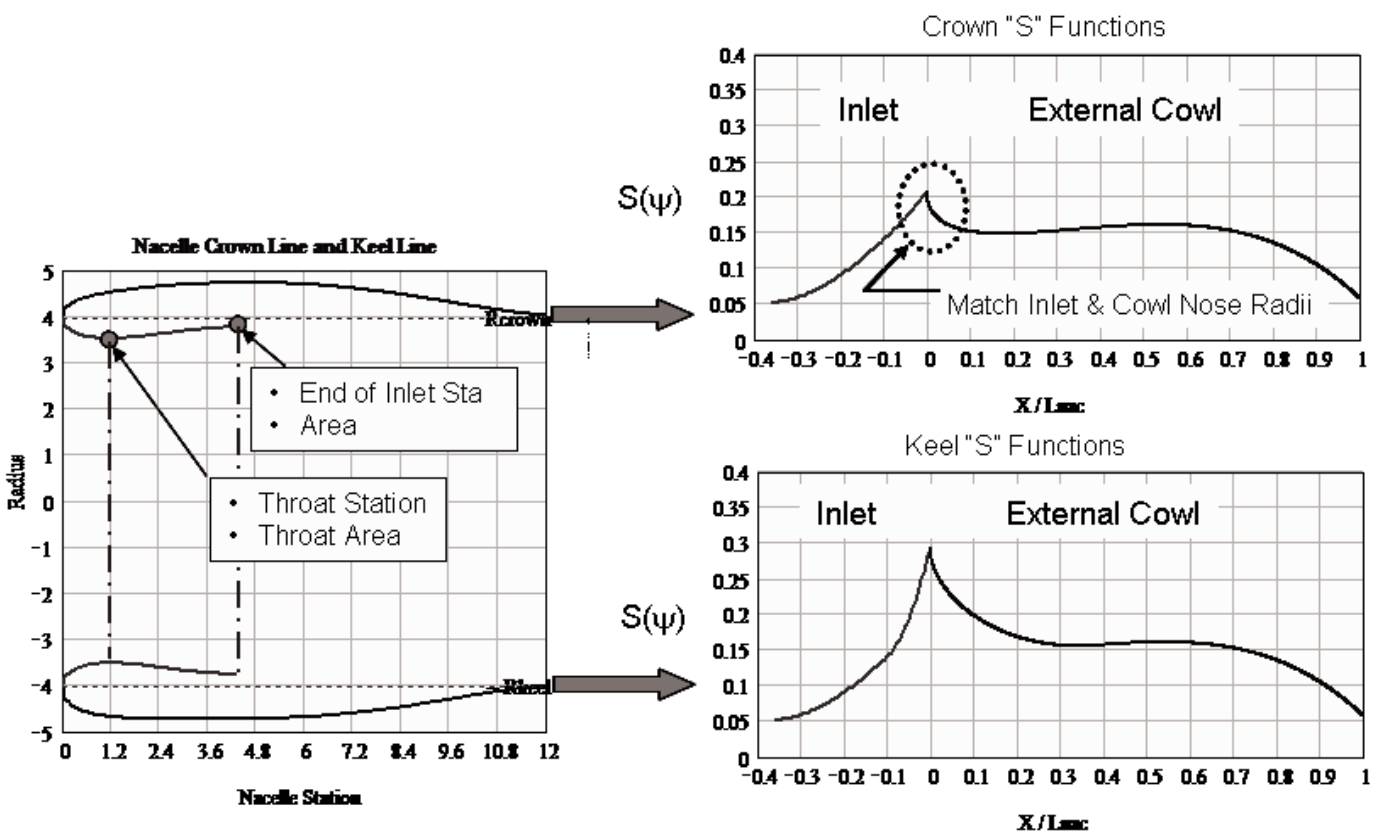

Figure 24. Nacelle inlet geometry definition ➔ 4 variables.

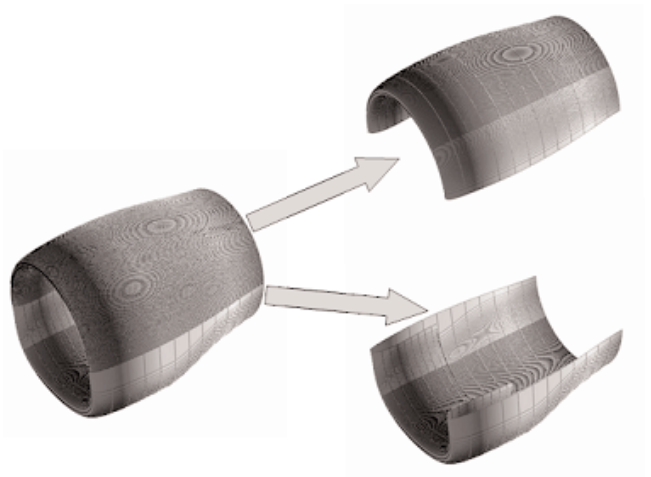

Figure 25. Total nacelle external shape and inlet geometry definition ➔ 15 variables.

Based on this example, it would appear that for aerodynamic design optimisation of the external shape of a nacelle, relatively few variables would be required to capture a very large design space of realistic smooth continuous geometries.

12.0 3D WING DEFINITION USING THE CST METHOD

A 3D wing can be considered to be a distribution of aerofoils across the wing span. Consequently we can use the previously discussed class functions and shape functions to obtain analytical definitions of the wing aerofoil sections and then simply distribute the analytical formulations across the wing span to completely define a wing. In this section the general analytical definition for any arbitrary wing will be developed. We will illustrate the use the methodology initially with a number of simple applications. This will be followed by an examination of application of the methodology to detailed subsonic and supersonic wings definitions.

A typical wing aerofoil section is shown in Fig. 26. The definition of a wing aerofoil section has two additional parameters relative to the previously shown aerofoil definition (Fig. 1)

The analytical definition of a local wing aerofoil section is similar to the aerofoil definition, (Equation (1)), with two additional parameters that include the local wing shear and wing twist.

$$\zeta_U(\psi,\eta) = \zeta_N(\eta) + C_{1\cdot0}^{0\cdot5}(\psi) S_U(\psi,\eta) + \psi\left[\zeta_T(\eta) - \mathrm{Tan}\left[\Delta\alpha_T(\eta)\right]\right] \quad \ldots (24)$$

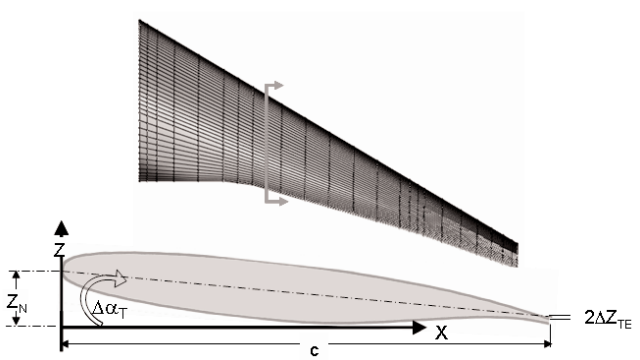

Figure 26. Wing aerofoil section.

Where:

Fraction of local chord: $\psi = \dfrac{x - x_{LE}(\eta)}{c(\eta)}$

Non-dimensional semi-span station: $\eta = \dfrac{2y}{b}$

Local leading edge co-ordinates: $x_{LE}(\eta)$

Local chord length: $c(\eta)$

Non-dimensional upper surface co-ordinate: $\zeta_U(\eta) = \dfrac{z_U(\eta)}{c(\eta)}$

Non-dimensional local wing shear: $\zeta_N(\eta) = \dfrac{z_N(\eta)}{c(\eta)}$

Local wing twist angle: $\Delta\alpha_T(\eta)$

Equation (24) is the equation for the wing upper surface, the similar equation for the lower surface is:

$$\zeta_L(\psi,\eta) = \zeta_N(\eta) + C_{1.0}^{0.5}(\psi) S_L(\psi,\eta) + \psi\left[\zeta_T(\eta) - \tan\left[\Delta\alpha_T(\eta)\right]\right] \quad \ldots (25)$$

The physical z co-ordinate is transformed in the shape function using an extension of the aerofoil shape function procedure to derive Equation (2). The corresponding shape for an aerofoil section on a wing with vertical shear and local section twist is given by the equation:

$$S_U(\psi,\eta) = \frac{\zeta_U(\psi,\eta) - \zeta_N(\eta) - \psi\left[\zeta_T(\eta) - \tan\left[\Delta\alpha_T(\eta)\right]\right]}{C_{1\cdot0}^{0\cdot5}(\psi)} \quad \ldots (26)$$

The corresponding shape function equation for the lower surface of a wing is:

$$S_L(\psi,\eta) = \frac{\zeta_L(\psi,\eta) - \zeta_N(\eta) - \psi\left[\zeta_T(\eta) - \mathrm{Tan}\left[\Delta\alpha_T(\eta)\right]\right]}{C_{1\cdot0}^{0\cdot5}(\psi)} \quad \ldots (27)$$

For a given wing definition, the wing upper and lower shape functions can be calculated using above equations.

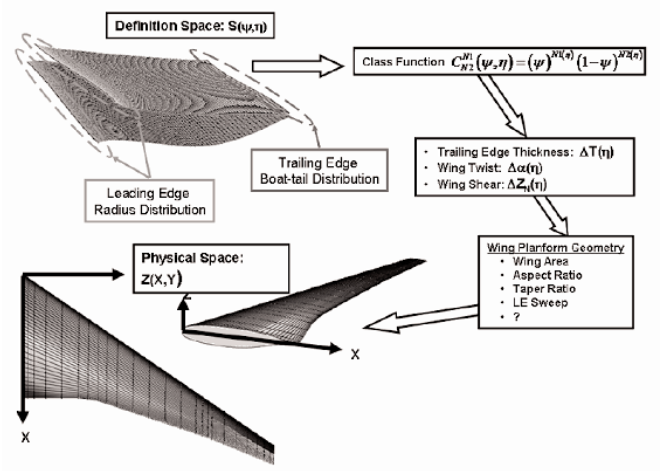

Figure 27. Definition of a wing in design space.

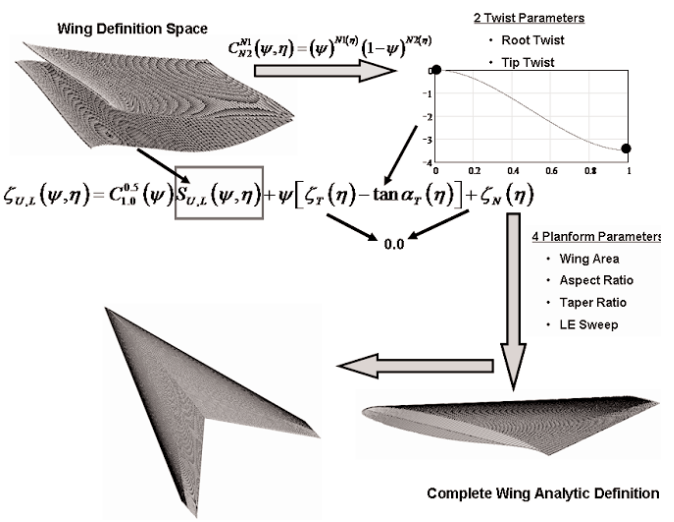

Figure 28. Complete wing analytic definition.

Given a wing definition as a shape function surface in the design space, the wing upper, and lower surfaces in physical space can be determined from the shape function surfaces, the local values of twist, shear and chord length as:

$$z_U(x,y)=\left\{\zeta_N(\eta)+C_{1\cdot0}^{0\cdot5}(\psi,\eta)S_U(\psi,\eta)+\psi\left[\zeta_T(\eta)-\mathrm{Tan}\left[\Delta\alpha_T(\eta)\right]\right]\right\}C_{LOCAL}(\eta)$$

$$z_L(x,y)=\left\{\zeta_N(\eta)+C_{1\cdot0}^{0\cdot5}(\psi,\eta)S_L(\psi,\eta)+\psi\left[\zeta_T(\eta)-\mathrm{Tan}\left[\Delta\alpha_T(\eta)\right]\right]\right\}C_{LOCAL}(\eta)$$

. . . (28)

A typical subsonic wing and the corresponding definition of the wing in the shape function design space is shown in Fig 27. The unit design space is defined by ψ = 0·0 to 1·0, and η = 0·0 to 1·0 and therefore represents any wing planform. As shown in the figure, the leading edges of the shape function surfaces define the leading-edge radius distributions for the physical wing. The trailing edges of the shape function surfaces define the boat-tail angle distributions. The wing shape function surface shares the same desirable features as the shape function for an aerofoil such as smooth, analytic, easily definable key geometric features.

The concept of the wing shape function surface can be used for many purposes including:

- Parametric wing definition
- Smoothing and/or enrichment of the wing geometry
- Local parametric changes of the wing geometry.
- Design optimisation with local design point variables
- Regional design optimisation such as the wing leading-edge region.
- Global design optimisation

Figure 28 illustrates the general process of transforming a simple parametric definition of shape function surfaces for a wing in design space into the physical definition of the wing.

The complete parametric cambered wing definition with spanwise variations of maximum thickness and wing twist, and specified wing area, sweep, aspect ratio and taper ratio required only a total of 19 design variables:

- Supercritical aerofoil section (11)
- Spanwise thickness variation (2)
- Spanwise twist variation (2)
- Wing area (1)
- Aspect ratio (1)
- Taper ratio (1)
- LE sweep (1)

13.0 MATHEMATICAL DESCRIPTION OF A WING IN DESIGN SPACE

Similar to the shape function for an aerofoil, the shape function surface for wings such as shown in Fig. 28, is a smooth continuous analytic surface. Consequently the shape function surface can be described by a Taylor series expansion in *x* and *y*. It was shown in Ref. 2 that a Taylor series in *x* and *y* is equivalent to a Taylor series expansion first in the *x* direction, and then expanding each coefficient of the '*x* series' as a Taylor expansion in the *y* direction. In a similar manner, it can be shown that a power series in *x* and *y* is equivalent to an expansion in *x* followed by power series expansions in the *y* direction of each of the *x* series co-efficients. Consequently, the shape function surface for a complete wing surface can be obtained by first representing the root aerofoil shape function by a Bernstein polynomial of a specified order.

The complete wing shape function surface can then be defined by expanding the co-efficients of the Bernstein in the spanwise direction using any appropriate numerical technique. The surface definition of the wing is then obtained by multiplying the shape function surface by the wing class function. This in essence provides a numeric scalar definition of the wing surface.

An example of the mathematical formulation of this process is shown below, using Bernstein polynomials to represent the stream wise aerofoil shapes as well as for the spanwise variation of the streamwise co-efficients.

The unit streamwise shape functions for Bernstein polynomial of order *Nx* are defined as:

$$Sx_i(\psi)=Kx_i\psi^i(1-\psi)^{Nx-i}\ \text{ for i = 0 to Nx} \qquad \ldots (29)$$

Where the streamwise binomial co-efficient is defined as

$$Kx_i\equiv\binom{Nx}{i}\equiv\frac{Nx!}{i!(Nx-i)!} \qquad \ldots (30)$$

The streamwise upper surface shape function at the reference spanwise station, η_{REF} is:

$$Su(\psi,\eta_{REF}) = \sum_{i=1}^{Nx} Au_i(\eta_{REF})\, Sx_i(\psi) \quad \ldots (31)$$

Let us represent the spanwise variation of each of the co-efficients, $Au_i(\eta)$ by Bernstein polynomials as:

$$Au_i(\eta) = \sum_{j=1}^{Ny} Bu_{i,j} Sy_j(\eta) \quad \ldots (32)$$

Where

$$Sy_j(\psi) = Ky_j \eta^j (1-\eta)^{Ny-j} \quad \text{for } j = 0 \text{ to } Ny \quad \ldots (33)$$

And

$$Ky_j \equiv \binom{Ny}{j} \equiv \frac{Ny!}{j!(Ny-j)!} \quad \ldots (34)$$

The wing upper surface is then defined by:

$$\zeta_U(\psi,\eta) = \sum_{i}^{Nx}\sum_{j}^{Ny} Bu_{i,j}\left\{C_{N2}^{N1}(\psi) Sy_j(\eta) Sx_i\right\} + \psi\left(\zeta_T(\eta) - \tan\alpha_{TWIST}(\eta)\right) + \zeta_N(\eta)$$

$$\ldots (35)$$

The similar equation for the lower surface is:

$$\zeta_L(\psi,\eta) = \sum_{i}^{Nx}\sum_{j}^{Ny} Bl_{i,j}\left\{C_{N2}^{N1}(\psi) Sy_j(\eta) Sx_i\right\} + \psi\left(\zeta_T(\eta) - \tan\alpha_{TWIST}(\eta)\right) + \zeta_N(\eta)$$

$$\ldots (36)$$

In Equations (35) and (36) the coefficients $Bu_{i,j}$ and $Bl_{i,j}$ define the unique geometry of the wing upper and lower surfaces. Continuity of curvature from the upper surface around the leading edge to the lower surface is easily obtained by the requirement: $Bu_{0,j}$ and $Bl_{0,j}$

The actual wing surface co-ordinates can then be obtained from the equations:

$$\begin{aligned} y &= \frac{b}{2}\eta \\ x &= \psi C_{LOC}(\eta) + x_{LE}(\eta) \\ z_U(x,y) &= \zeta_U(\psi,\eta) C_{LOC}(\eta) \\ z_L(x,y) &= \zeta_L(\psi,\eta) C_{LOC}(\eta) \end{aligned}$$

$$\ldots (37)$$

This process of defining a wing geometry using Equations (35) to (37), may be considered a scalar loft of a wing where every point on the wing surface is defined as accurately as desired and the points are all 'connected' by the analytic equations. This is in contrast to the usual wing definition of a vector loft of a wing which is defined as ordered sets of *x,y,z* co-ordinates plus 'rules' that describe how to connect adjoining points. The common approach used to connect adjacent points is along constant span stations and along constant percent chord lines.

In Equations (35) and (36), each term $\zeta_{ij}(\psi,\eta) = C_{N2}^{N1}(\psi) Sy_j(\eta) Sx_i(\psi)$ defines a composite wing geometry formed by the 'ith' component aerofoil shape $C_{N2}^{N1}(\psi) Sx_i(\psi)$ with the 'jth' spanwise variation $Sy_j(\eta)$. Figure 29 shows analytic wing components for an arrow wing with a

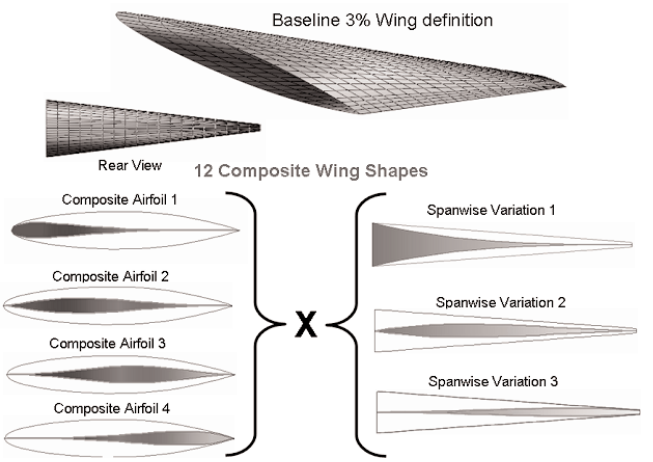

Figure 29. Arrow wing composite wing elements construction.

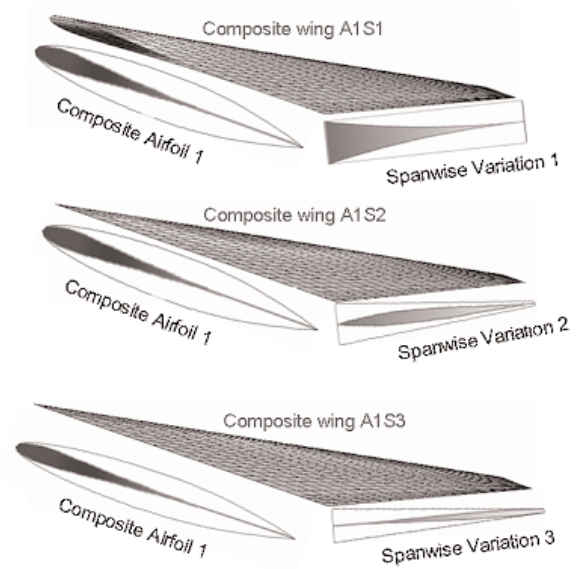

Figure 30. Example composite wing elements.

Bernstein polynomial of order 3 for defining the basic aerofoil shape and Bernstein polynomial of order 2 for describing the spanwise variations for each of the basic aerofoil components. This results in a total of 12 component wing shapes used to define the complete wing geometry. Figure 30 shows three of the component wing shapes.

For a design optimisation application, the 12 scaleable coefficients Bij would be the optimisation variables.

Figure 31 shows an example of a scalar loft of a highly swept wind tunnel configuration that was used to obtain surface pressure and wings loads data for CFD validation studies[13, 14]. The wind-tunnel model was built using the conventional vector loft approach.

The analytic scalar loft of the wing was defined by a total of 15 parameters. These include:

- BPO8 representation of the basic aerofoil section ➔ nine parameters
- Wing area
- Aspect ratio
- Taper ratio
- Leading-edge sweep
- Trailing-edge thickness = constant

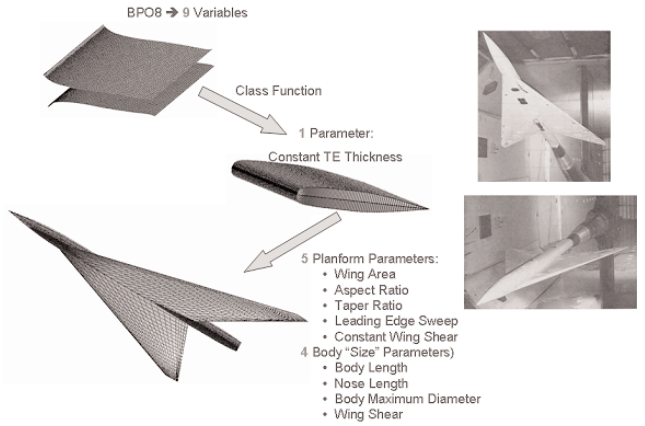

Figure 31. Scalar loft of a highly swept aero-elastic loads wind tunnel model.

- Constant wing shear (to fit the wing on the body as a low wing installation)

The wind tunnel model fuselage included an ogive nose/cylindrical body. The ogive nose shape has distribution class function with exponents equal to 1 and a constant shape function equal to four times the maximum body radius. The total body geometry was specified by two variables that included the nose length and the maximum radius.

Body and wing surface coordinates were calculated using the aforementioned analytic definition. The differences between the analytic model surface definition and the 'as built' wing surface coordinates were far less than wind-tunnel model tolerances over the entire surface of the model.

14.0 MATHEMATICAL DESCRIPTION OF A WING WITH LEADING-EDGE AND/OR TRAILING-EDGE BREAKS

Subsonic and supersonic aircraft wings typically have planform breaks in the leading-edge (commonly called a strake) and/or the trailing-edge (commonly called a yehudi) with discontinuous changes in sweep. Consequently, the wing surface is non-analytic in the local region of the edge breaks. However, the approach of defining a complete wing geometry as previously described should be piecewise applicable.

In order explore this concept; the geometry of a typical subsonic aircraft wing was analysed in depth. Aerofoil sections at a large number of spanwise stations were approximated by equal order of Bernstein polynomial representation of the corresponding shape functions. The adequacy of the composite representation was determined by computing the residual differences between the actual aerofoil sections and those defined by the approximating Bernstein polynomials. The wing upper and lower surface residual differences were well within the wind-tunnel model construction tolerances.

The shape function surfaces corresponding to wing upper and lower surfaces are shown in Fig. 32. The piecewise continuous nature of the surfaces associated with the planform breaks is very evident. The corresponding spanwise variations of the composite aerofoil scaling coefficients (Bu_j and Bl_j) are also shown.

These results show that the spanwise variations of the Bernstein coefficients across the wing span are very regular, piecewise continuous and well behaved.

The shape function surface for a High Speed Civil Transport, Ref. H, wing is shown in Fig. 33. This planform has a number of leading edge and trailing-edge breaks. This wing has an inboard subsonic leading edge wing with round nose aerofoils. Outboard of the

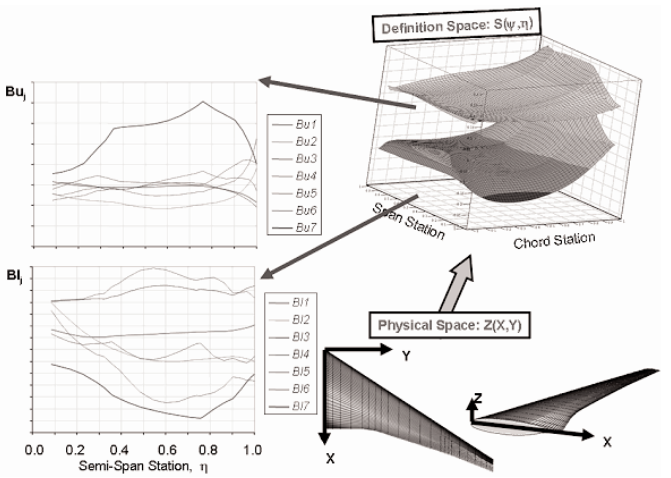

Figure 32. Spanwise variation of the 'BP' composite aerofoil scaling co-efficients.

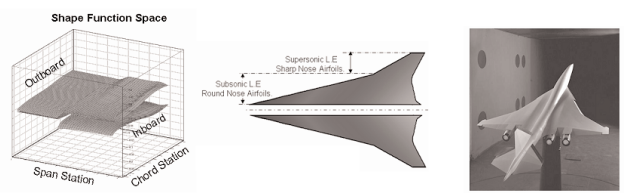

Figure 33. Shape function for a HSCT supersonic wing – Ref H.

leading edge the wing has a supersonic leading edge with sharp nose aerofoils. The shape functions for this wing are also seen to be piecewise smooth and continuous.

The results shown in Figs 32 and 33 imply indicate that analytic wing definitions for planforms with leading-edge and/or trailing-edge breaks, can be developed using streamwise aerofoil components for a fixed order of Bernstein polynomials with piecewise variations of the polynomial coefficients in the spanwise direction.

15.0 ANALYTIC WING GLOBAL DESIGN OPTIMISATION

In Ref. 15, a new supersonic linear theory wave drag optimisation methodology utilising far field wave drag methodology was introduced. The optimisation process was used to explore wing design optimisation with the class function/shape function transformation, CST, concept of an analytic scalar wing definitions.

Results of a simple application of the methodology for optimisation of the spanwise thickness distribution of a supersonic delta wing at Mach 3.0 to minimise cruise volume wave drag, are shown in Figs 34 to 36.

The objective of the study was to explore the effect of the order of the spanwise Bernstein polynomial representation of the wing shape function surface with a constant aerofoil shape on wave drag with a constant wing volume. The basic wing/body geometry characteristics of the base configuration are shown in Fig 34.

Similar to the arrow wing analytic representation shown in Fig. 29, the study wing geometry was decomposed into scaleable component wing shapes formed by the different spanwise variations of the basic wing aerofoil shape. The component wing shapes, corresponding to a 3rd order Bernstein polynomial describing the spanwise thickness variation, are shown in Fig 35.

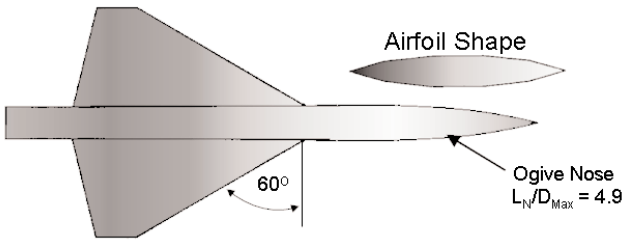

Figure 34. Basic delta wing/body.

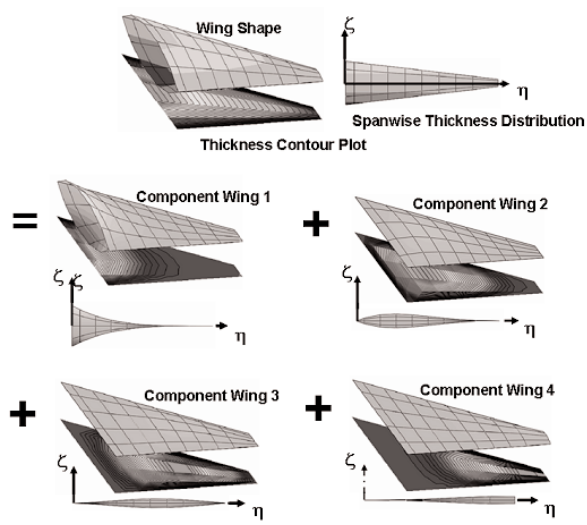

Figure 35. Example of BP03 spanwise analytic wing components.

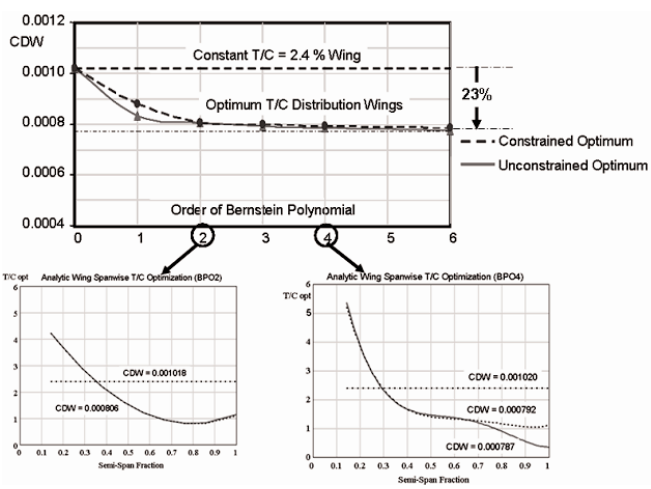

Figure 36. Effect of Spanwise bernstein polynomial order ~ BPO, on optimized wing wave drag.

Wing optimisation studies were conducted with and with out outboard wing inequality thickness constraints. The thickness constraints limited the outboard thickness to no less than 1·1%. In all cases the wing volume was held constant. Spanwise Bernstein polynomials of order, BPO 0 to 6 were utilised to define the composite wing shapes for the optimisation studies. The results of the study are summarised in Fig. 36.

The number of design optimisation variables corresponding to scaling coefficients of the component wing shapes equals the BPO plus 1. The BPO = 0 result corresponds to the drag of the constant T_{MAX}/C = 2·4% baseline wing. It is seen that the wave drag rapidly converges to the minimum drag level when the BPO representation equals or exceeds 2. For this example the wing wave drag was reduced by 23%. Additional results of design optimisation studies that demonstrate the effectiveness of the analytic optimisation methodology using composite wings representing both aerofoil shape and spanwise thickness variations over the wing surface are shown in Reference 15.

16.0 SUMMARY AND CONCLUSIONS

Figure 37 summaries the evolution of the CST method as presented in this report.

- The concept of the 'SHAPE FUNCTION' was developed by a transformation process that eliminated the numerical leading edge singularities in slopes, 2nd derivatives and the large variations in curvature over the entire surface of an aerofoil. In addition, the shape function provides direct control of key design parameters such as leading-edge radius, continuous curvature around a leading edge, boat-tail angle and closure to a specified thickness.
- The transformation process was generalised with the introduction of the 'CLASS FUNCTION'.
- The class function defines fundamental classes of aerofoils, axi-symmetric bodies, and axi-symmetric nacelles geometries. The shape function defines unique geometric shapes within each fundamental class.
- The unit shape function was decomposed into component aerofoils using Bernstein Polynomials. This is an attractive and systematic technique to decompose the basic unit shape into scalable elements corresponding to discrete component aerofoils.
- By virtue of the Weirstrass theorem it was shown that this technique:
- Captures the entire design space of smooth aerofoils, axi-symmetric bodies and nacelles
- Within this design space, all smooth aerofoils, axi-symmetric bodies and nacelles are derivable from the unit shape function and therefore from each other.
- Very detailed geometric and aerodynamic evaluations were made of approximate aerofoil geometries derived from various orders of Bernstein polynomials representations of the shape functions for a wide variety of aerofoil geometries. The results indicated that relatively few variables were required to accurately represent most any aerofoil geometry.
- The CST methodology can be readily adapted to describe both warping and morphing of geometric components. Geometric morphing can be easily obtained by variations of class function/shape function variables. Warping involves geometric variations external to the class function/shape function variables.
- The **C**lass function/**S**hape function **T**ransformation geometry representation methodology, CST, can be used to describe both the cross-sectional shapes of arbitrary bodies or nacelles as well as the distribution of the cross-section shapes along the primary body axis. This provides a powerful technique to smoothly morph a three dimensional geometry into widely differing configuration.
- The concept of 'analytic scalar definitions using composite wing surfaces' was introduced and explored. With this approach, the wing aerofoil shapes functions are represented

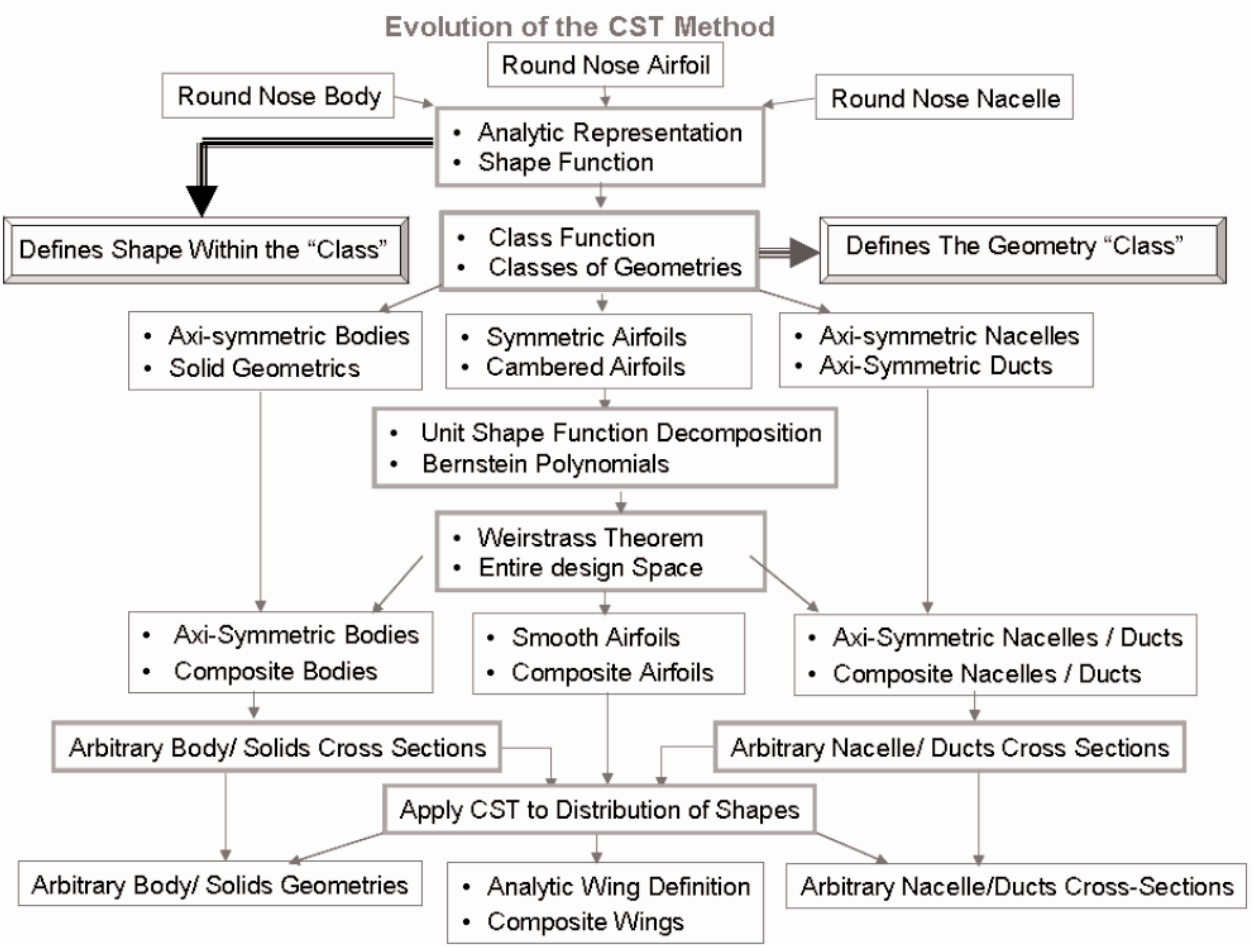

Figure 37. Evolution of the CST method.

by a Bernstein polynomial. The selected order of Bernstein polynomial effectively defines a set of composite aerofoils. The scalable coefficients of the composite aerofoils can than be mathematically expanded in the spanwise direction to define a set of composite wing shapes.

- The complete wing upper and lower shape function surfaces can then defined by scaling the set of composite wing shapes as the variables for design optimisation applications and parametric design studies. The concept of the wing shape function surface can be used for many purposes including:
  - Parametric wing and body definitions
  - Smoothing and/or enrichment of the wing or body geometries.
  - Local parametric changes of the wing geometry.
  - Defining seeming complex geometries with relatively few variables
- Aerodynamic and multi-disciplinary design optimisation, MDO, studies with relatively few required design variables
- Local area design optimisation such as the wing leading edge region.
- The analytic CST geometry representation methodology presented in this report provides a unified and systematic approach to represent a wide variety of 2D and 3D geometries encompassing a very large design space with a relatively few scalar parameters.

REFERENCES

1. KULFAN, B.M. and BUSSOLETTI, J.E. Fundamental parametric geometry representations for aircraft component shapes, AIAA-2006-6948, 11th AIAA/ISSMO Multidisciplinary analysis and optimisation conference: the modeling and simulation frontier for multidisciplinary design optimisation, 6-8 September, 2006.
2. KULFAN, B. M. Universal parametric geometry representation method – 'CST', AIAA-2007-0062, 45th AIAA Aerospace sciences meeting and exhibit, January, 2007.
3. SOBIECZKY, H. Aerodynamic design and optimisation tools accelerated by parametric geometry preprocessing, European congress on computational methods in applied sciences and engineering, ECCOMAS, 2000.
4. SOBIECZKY, H. Parametric aerofoils and wings, notes on numerical fluid mechanics, *Vieweg Verlag*, **68**, 1998, pp 71-88.
5. SAMAREH, J.A. Survey of shape parameterisation techniques for high-fidelity multidisciplinary shape optimisation, *AIAA J,* May 2001, **39,** (5).
6. ROBINSON, G.M. and KEANE, A.J. Concise orthogonal representation of supercritical aerofoils, *J Aircr*, **38,** (3).

7. SONG, W. and KEANE, A. J. A study of shape parameterisation aerofoil optimisation, AIAA-2004-4482 10th AIAA/ISSMO Multidisciplinary analysis and optimisation conference, Albany, New York, 30 August - 1 September, 2004.
8. PADULA, S. and LI, W. Options for robust aerofoil optimisation under uncertainty, 9th AIAA multidisciplinary analysis and optimisation symposium, 4-6 September 2002.
9. HICKS, R.M. and HENNE, P.A. Wing design by numerical optimisation, *J Aircr*, 1978, **15,** pp 407-412.
10. PADULA, S. and LI, W. Options for robust aerofoil optimisation under uncertainty, 9th AIAA multidisciplinary analysis and optimisation symposium, 4-6 September 2002.
11. PURCELL, T.W. and OM, D. TRANAIR packaging for ease-of-use in wing design, AIAA-1998-5575, AIAA and SAE, 1998 world aviation conference, Anaheim, CA, 28-30 September, 1998.
12. SAMANT, S.S., BUSSOLETTI, J.E., JOHNSON, F.T., BURKHART, R.H., EVERSON, B.L., MELVIN, R.G., YOUNG, D.P., ERICKSON, L.L. and MADSON, M.D. TRANAIR – A computer code for transonic analyses of arbitrary configurations, AIAA-1987-34, 25th Aerospace sciences meeting, Reno, NV, 12-15 January, 1987.
13. MANRO, M.E., BOBBITT, P.J. and KULFAN, R.M. The prediction of pressure distributions on an arrow wing configuration including the effects of camber twist and a wing fin, NASA CP-2108, November 1979, Paper No 3, pp 59 to 115.
14. WERY, A.C. and KULFAN, R.M. Aeroelastic loads prediction for an arrow wing – task II evaluation of semi-empirical methods, NASA CR-3641, March 1983.
15. KULFAN, B.M. A new supersonic wing far-field composite element wave drag optimisation method, FCE, AIAA-2008-0132, 46th AIAA aerospace sciences meeting and exhibit, January 2008.